Slot coating flows of non-colloidal particle suspensions

Journal:	*AIChE Journal*
Manuscript ID	AIChE-16-17675.R1
Wiley - Manuscript type:	Research Article
Date Submitted by the Author:	16-May-2016

Complete List of Authors:	Valdez Silva, Luis; PUC-Rio, Department of Mechanical Engineering Campana, Diego; Instituto de Desarrollo Tecnologico para la Industria Quimica - CONICET Carvalho, Marcio; PUC-Rio, Department of Mechanical Engineering

Keywords:	free surface flow, slot coating, particle suspension

Slot coating flows of non-colloidal particle suspensions

L. D. Valdez Silva[b], D. M. Campana[a], M. S. Carvalho[b,*]

[a]*Instituto de Desarrollo Tecnológico para la Industria Química, CONICET, Güemes 3450, Santa Fe, 3000, República Argentina*
[b]*Department of Mechanical Engineering, Pontificia Universidade Catolica do Rio de Janeiro, Rua Marques de Sao Vicente 225, Gavea, Rio de Janeiro, RJ, 22453-900, Brazil*

Abstract

Slot coating is used in the manufacturing of functional films, which rely on specific particle microstructure to achieve the desired performance. Final structure on the coated film is strongly dependent on the suspension flow during the deposition of the coating liquid and on the subsequent drying process. Fundamental understanding on how particles are distributed in the coated layer enables optimization of the process and quality of the produced films.

The complex coating flow leads to shear-induced particle migration and non-uniform particle distribution. We study slot coating flow of non-colloidal suspensions by solving the mass and momentum conservation equations coupled with a particle transport equation using the Galerkin/Finite element method. The results show that particle distribution in the coating bead and in the coated layer is non-uniform and is strongly dependent on the imposed flow rate (wet thickness).

Keywords:

*Corresponding author. Email address: msc@puc-rio.br

Preprint submitted to AIChE Journal *May 16, 2016* free surface flow, slot coating, particle suspension

1. Introduction

Many coated products, such as anti-reflection, hydrophobic films and flexible electrodes, rely on a designed microstructure in order to achieve the desired functionality. One way of mass producing functional coated films is by depositing a particle suspension onto a moving substrate and subsequently drying the liquid to form the final solid film. The final microstructure of the coated layer is directly affected by the suspension flow during the coating and drying processes, due to particle migration effects. Cardinal et al.[1] have shown how the relative strength of liquid evaporation, particle diffusion and sedimentation affect the particle distribution on the coated film during drying. A 1-D particle conservation equation was used to describe the particle concentration evolution during drying by taking into account for the aforementioned effects, while cryo-electron microscopy images were used to validate the predicted drying map. However, the model assumes that the particle concentration is uniform through the thickness of the film in the initial stages of drying. This may not be the case when the liquid film is deposited on the substrate by slot coating process, for example, where high shear rate gradient are developed in the coating bead.

If the suspended particles are large enough, Brownian motion, van der Walls and electrical double layer forces between particles can be neglected and the resulting liquid is a non-colloidal suspension. In this condition, the suspension viscosity becomes a function of the particle volume fraction only.[2,3,4,5] When this suspension is set in non-uniform flow (as those mostly encountered in coating processes), particles are transported by convection, sedimentation/buoyancy and shear rate and viscosity gradient driven diffusion. The last two mechanisms are frequently called *shear-induced* particle migration. This behavior was described, for example, in the suspension flows inside cylindrical tubes[6] and in the Coutte flow between concentric cylinders.[7] The main observation was that particles migrate from regions with higher to lower shear rate. Later, Leighton and Acrivos[8] developed a rational explanation for these mechanisms based on the frequency of the inter-particle collisions and the effective viscosity of the suspension, both being functions of the non-uniform local particle volume fraction. This phenomena has been confirmed experimentally in different situations.[9,10]

Based on the work of Leighton and Acrivos,[8] Phillips et al.[11] proposed a convective-diffusion equation that describes the particle concentration variation in laminar flows. This approach was called diffusive flux model and depends on two diffusion parameters, which they considered as constants to be fitted using experimental results. By considering the fluid as Newtonian, but with the viscosity being function of the local particle concentration, Phillips et al.[11] solved the particle transport equation coupled with the momentum conservation for two flow configurations: Poiseuille pressure driven flow in a circular tube and Couette flow between rotating cylinders. The diffusive flux model was also successfully used in different analyses.[12,13,14] However, the model cannot correctly predict the radial particle migration of some viscometric flows and different improvements and corrections have been proposed. For example, Krishnan et al.[15] suggested that the curvature of streamlines also contributes to the radial particle migration. More recently, Kim et al.[16] developed a model to take into account this curvature-induced particle flux. Tetlow et al.[17] also suggested that the diffusion parameters of the model should depends on the local particle concentration.

Another approach to study particle migration in flows of concentrated suspensions is the Suspension Balance Model, which was first proposed by Nott and Brady.[18] Its physical concept is that the migration phenomenon arises in order to balance a non-homogeneous normal stress that exists due to the presence of the particles. The particle flux is directly proportional to the divergence of the particle stress tensor (i.e., an additional stress in the fluid phase stress tensor). They show that in a simple shear flow, the suspension balance model leads to a diffusion equation of the same form as the one obtained with the diffusive flux model.

Despite its limitations, the original diffusive flux model[11] is relatively simple to implement in computational codes and has been used to study more complex flows. For example, Ritz et al.[19] used the model to calculate the particle distribution inside a short-dwell coater, Rao et al.[20] to describe instabilities on bath sedimentation problems and Ahmed and Singh[21] implemented the model to calculate the particle distribution downstream a bifurcation channel. We apply the model to study steady slot coating flow of particle suspensions.

Particle migration has tremendous impact on rheological measurements of particle suspensions [22, 23, 24] and on different process flows of slurries [25, 26]. The effect of particles is also even more pronounced when the flow has free surfaces, as discussed by Timberlake and Morris[27] and Furbank and Morris[28] on the drop formation and pinch-off of pendant/ejected drops. The non-uniform particle distribution that leads to viscosity variation within the flow triggers different flow instabilities.

Despite its fundamental importance in fluid mechanics and industrial applications, analysis of coating flows of particle suspension that takes into account particle migration mechanisms is still rare in the literature. One usual approach is to consider the liquid as a Newtonian or a shear-thinning fluid using the viscosity (or viscosity curve) evaluated at the average particle concentration. However, the complex flow in the coating bead may lead to particle migration and non uniform particle distribution downstream of the film formation region. An alternative approach is to study particle distribution in the flow assuming that the flow is not affected by the particles.[29]

Up to our knowledge, there is no experimental measurements of particle distribution in the liquid coated film. Theoretical and numerical analyses are also rare. The only exception for a two-way coupling between flow and particle transport is the work of Min and Kim[30] who studied numerically, using the finite volume method, the effect of particle migration in two free surface flows. Using the diffusive flux model,[11] they first computed the flow field and particle distribution in a planar liquid jet ejected from two parallel plates, obtaining results for different particle sizes, mean particle concentrations and Reynolds numbers. They also solved the flow for a slot coating configuration, but due to convergence problems in the numerical technique used, the range of operation parameters explored was limited.

The aim of this work is to study slot coating flow of non-colloidal particle suspension for flow conditions typically encountered in industrial applications. The steady-state, two-dimensional momentum, mass conservation and the particle transport equations for the free boundary problem were solved in a fully coupled scheme using the Galerkin/Finite element method. The effect of particle migration on the steady flow states is the first step towards a fundamental understanding on how the presence of particles suspended in the coating liquid can affect the operating window of the process, i.e. the conditions at which the flow becomes transient or three-dimensional. The steady-state solutions presented here can be used as base state for stability analysis of the flow.

The paper is organized as follow: section 2 presents the governing equations and boundary conditions for the fluid flow problem (section 2.1) and particles transport (section 2.2); the numerical technique is explained in sections 3.1 and 3.2, while validation results are discussed in section 3.3. Finally, section 4 presents the new results and section 5 is devoted for the final remarks.

2. Mathematical formulation

In slot coating process, the liquid is pumped to a coating die in which an elongated chamber distributes it across the width of a narrow slot. Exiting the slot, the liquid fills (wholly or partially) the gap H_0 between the adjacent die lips and the substrate translating rapidly past them at a speed V_s. The liquid in the gap, bounded upstream and downstream by gas-liquid interfaces, or menisci, forms the coating bead, as shown in Fig. 1. In order to sustain the coating bead at higher substrate speeds and smaller wet thickness, the gas pressure at the upstream meniscus is made lower than ambient, i.e. a slight vacuum p_{vac} is applied to the upstream meniscus. The

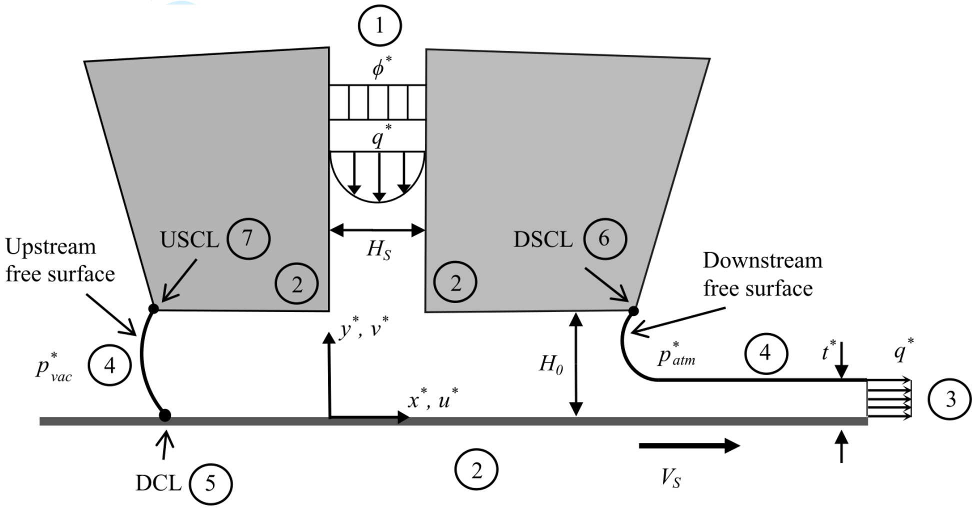

Figure 1: Sketch of the slot coating head, moving substrate and coated film. The boundaries are denoted by number according the imposed boundary conditions.

upstream meniscus is bounded by the upstream contact line (USCL in Fig.1) and the dynamic contact line (DCL) where the liquid wets the moving substrate. The downstream meniscus starts at the downstream static contact line (DSCL in Fig.1). Slot coating belongs to a class of coating methods known as *pre-metered coating*: the thickness t of the coated layer is set by the flow rate fed to the coating die q and the speed of the moving substrate, and is independent of the other process variables, i.e. $t = q/V_s$.

2.1. Governing equations for fluid flow

In this work we neglect both the inertial and gravitational effects based on the fact that the flow dimension is very small, e.g. $H_0 \approx 100\mu$m. Thus, the velocity $\mathbf{v} = u\mathbf{i} + v\mathbf{j}$ and pressure p fields of the two-dimensional and steady Stokes flow are governed by the continuity and momentum equations for incompressible liquid:

$$\nabla \cdot \mathbf{v} = 0 \tag{1}$$

$$\nabla \cdot \mathbf{T} = \nabla \cdot [-p\mathbf{I} + \tau] = 0 \tag{2}$$

The parameter η_s represents the constant dynamic viscosity of the solvent. Because we are considering non-colloidal suspensions, the viscous stress τ is taken to be a linear function of the rate-of-strain tensor. The viscosity of the suspension is only a function of the local particle concentration ϕ and does not vary with the deformation rate:

$$\begin{gathered} \tau = \eta(\phi)\underline{\underline{\dot{\gamma}}} \\ \underline{\underline{\dot{\gamma}}} = \nabla\mathbf{v} + \nabla\mathbf{v}^T \end{gathered} \tag{3}$$

The relative viscosity of the suspension is defined as $\eta_r(\phi) = \eta(\phi)/\eta_s$. According to the empirical observation of Krieger,[31] the relative viscosity of a non-colloidal suspension (high Péclet number, $Pe \gg 1$) is well approximated by

$$\eta_r = (1 - \phi^*)^{-1.82}, \tag{4}$$

where $\phi^* = \phi/\phi_m$ is the relative particle volume fraction, being ϕ_m the *maximum packing concentration.*

The relative viscosity of the suspension η_r approaches infinity as the particle concentration approaches the maximum packing concentration, which for rigid spheres is $\phi_m \sim 0.68$. Although Eq.(4) was originally proposed for suspensions with $0.01 < \phi < 0.5$, we follow the same approach of Phillips et al.[11] and consider that it is valid for $0.01 < \phi < 0.68$.

The following boundary conditions are applied to the momentum conservation equation; the boundaries are identified by corresponding numbers in Fig. 1:

1. At the inflow of the feed slot, the flow is fully developed and the velocity profile given by

$$\mathbf{v} = -6V_s t \left[(x/H_s) - (x/H_s)^2\right] \mathbf{j}, \tag{5}$$

   where V_s is the substrate speed, t is the film thickness and H_s the width of the feed channel.

2. Along the solid surfaces, no-slip and no penetration conditions are applied

$$\mathbf{v} = 0, \text{ along feed channel and slot die walls}$$
$$\mathbf{v} = \mathbf{i}, \text{ along substrate} \tag{6}$$

3. Along the outflow plane, the flow is assumed to be fully developed and the pressure is set to the ambient pressure p_{amb}:

$$\mathbf{n} \cdot \nabla \mathbf{v} = 0$$
$$p = p_{amb} \tag{7}$$

In this work, the constant ambient pressure is arbitrary set as $p_{amb} = 0$.

4. Along the free surfaces, the kinematic condition and force balance are applied:

$$\mathbf{n} \cdot \mathbf{T} = (\sigma\kappa - p_{amb})\,\mathbf{n} \tag{8}$$

$$\mathbf{n} \cdot \mathbf{v} = 0, \tag{9}$$

where $p_{amb} = 0$ and $p_{amb} = p_{vac}$ on the downstream and upstream free surfaces, respectively. In addition, $\kappa = -\nabla_s \cdot \mathbf{n}$ is the interface curvature, $\nabla_s = (\nabla - \mathbf{nn})$ the surface gradient operator, $\mathbf{n}$ the outward unit normal vector, and σ is the surface tension of the liquid.

5. At the dynamic contact line (DCL), the stress singularity is removed by applying the Navier's slip condition (see for example[32]) and a constant contac angle is set:

$$(1/\beta)\mathbf{i} \cdot (\mathbf{v} - \mathbf{i}) = \mathbf{i} \cdot (\mathbf{T} \cdot \mathbf{n}) \tag{10}$$

$$\mathbf{n}_w \cdot \mathbf{n}_f = \cos(\theta_d), \tag{11}$$

where β is the slip coefficient, $\mathbf{n}_w$ is the normal vector to the solid wall directed into the fluid and $\mathbf{n}_f$ is the outward normal vector to the free surface

6. The DSCL is fixed at the edge of the die lip; then both x and y-coordinate are fixed

$$\mathbf{x}_{dscl} = \mathbf{x}_{edge} \tag{12}$$

7. Finally, the USCL is free to move along the die lip and therefore it have always the same y-coordinate

$$\mathbf{j} \cdot \mathbf{x}_{uscl} = 1 \tag{13}$$

We also set an upstream static contact angle, θ_s, as in Eq. (11).

2.2. Governing equations for particle transport

In this work we used the model proposed by Phillips et al.[11] to describe particle transport in the suspension flow. The model, in steady state condition, considers that particles are transported by convection and diffusion mechanisms. Then, the general conservation equation for the particle volume fraction is

$$\nabla \cdot (\phi \mathbf{v}) + \nabla \cdot (\mathbf{N}_t) = 0, \tag{14}$$

where $\mathbf{N}_t$ is the total particle flux that accounts for Brownian diffusion, sedimentation, shear and viscosity gradients induced transport. Under the hypothesis of non-colloidal suspension and neutrally buoyant particles, the first two mechanisms are neglected. Therefore, we only consider here the fluxes induced by shear rate and viscosity gradients, which according to Phillips et al.[11] are given by:

$$\mathbf{N}_t = \mathbf{N}_\phi + \mathbf{N}_\eta \tag{15}$$

$$\mathbf{N}_\phi = -k_c a^2(\phi^2\nabla\dot{\gamma} + \phi\dot{\gamma}\nabla\phi) \tag{16}$$

$$\mathbf{N}_\eta = -k_\eta\dot{\gamma}\phi^2\left(\frac{a^2}{\eta_r}\right)\frac{d\eta_r}{d\phi}\nabla\phi. \tag{17}$$

k_c and k_η are constants of order unity, which must be determined by experiments, a is the particle radius and $\dot{\gamma}$ is *the deformation rate* or simply *shear rate*.[33] It is defined as

$$\dot{\gamma} = \sqrt{\frac{1}{2}\mathrm{tr}(\underline{\underline{\dot{\gamma}}}^2)} = \tag{18}$$

$$= \left[2\left(\frac{\partial u}{\partial x}\right)^2 + 2\left(\frac{\partial v}{\partial y}\right)^2 + 2\left(\frac{\partial u}{\partial y} + \frac{\partial v}{\partial x}\right)^2\right]^{1/2} \tag{19}$$

The final transport equation is obtained after replacing Eqs. (15) to (17) in Eq. (14):

$$\mathbf{v}\cdot\nabla\phi = \nabla\cdot(\bar{D}\nabla\phi) + k_c a^2\nabla\cdot(\phi^2\nabla\dot{\gamma}), \tag{20}$$

where

$$\bar{D} = k_c a^2\phi\dot{\gamma} + k_\eta\dot{\gamma}\phi^2\frac{a^2}{\eta}\frac{d\eta}{d\phi} \tag{21}$$

The boundary conditions applied to solve Eq. (20) are:

1. At the feed slot, we consider a constant concentration profile with $\phi = \bar{\phi}$, where $\bar{\phi}$ the *average bulk concentration* of the suspension.
2. The solid walls are impermeable and then the particle flux is set to zero: $\mathbf{n} \cdot \mathbf{N}_t = 0$.
3. At the outflow plane, we impose a fully developed flow condition: $\mathbf{n} \cdot \mathbf{N}_t = 0$.
4. Finally, because in this work we do not consider adsorption/desorption at interfaces, the particle flux is also set to zero along the free surfaces.

In the finite element method, the velocity field is usually written as a linear combination of continuous piece-wise polynomials. Therefore, along element boundaries, the velocity $\mathbf{v}$ is continuous, but the velocity gradient $\nabla \mathbf{v}$ is not. Therefore, the weighted residual of the particle transport equation, which includes the integral of the gradient of deformation rate $\nabla \dot{\gamma}$ cannot be evaluated. A common approach to avoid this problem is to represent the velocity gradient as a separate independent field which is defined also as a linear combination of continuous piece-wise polynomials. Thus, an additional variable $\mathbf{G} = \nabla \mathbf{v}$ that is continuous between the elements is introduced and it is called *interpolated velocity gradient*. This is the same approach used in the solution of viscoelastic flows using finite element method (see Szadi et al.[34]).

The approximate solution satisfies the continuity equation only in an integral sense, $\mathrm{tr}(\mathbf{G}) = \nabla \cdot \mathbf{v} = 0$ is not satisfied in every point of the flow domain. Pasquali and Scriven[35] suggested that the interpolated velocity gradient field $\mathbf{G}$ can be defined such that the incompressibility constrain is automatically enforced, i.e. $\mathrm{tr}(\mathbf{G}) \equiv 0$. The proposed definition is:

$$\mathbf{G} - \nabla \mathbf{v} + \frac{\nabla \cdot \mathbf{v}}{\mathrm{tr}(\mathbf{I})}\mathbf{I} = \mathbf{0} \tag{22}$$

Note that $\mathrm{tr}(\mathbf{G}) = \mathrm{tr}(\nabla \mathbf{v}) - \nabla \cdot \mathbf{v} = 0$.

In the next section we present the numerical method used to discretize and solve the free boundary problem defined by Eqs. (1), (2), (20) and (22).

The governing equations are made dimensionless by using V_s, H_0, H_0/V_s and $V_s\eta_s/H_0$ as scales for velocity, length, time and stress, respectively.

3. Numerical Solution

3.1. Formulation of the free boundary problem

In coating flows, the domain Ω (with boundaries Γ) is unknown *a priori* due to the presence of the free surfaces. Thus, to solve this free boundary problem by standard techniques, the set of differential equations and boundary conditions have to be transformed to an equivalent set defined in a known reference domain $\overline{\Omega}$ (with boundaries $\overline{\Gamma}$). This can be done by using a mapping $\mathbf{x} = \mathbf{x}(\boldsymbol{\xi})$ between the two domains. The unknown physical domain is parameterized by the position vector $\mathbf{x}$ and the reference domain, by the vector $\boldsymbol{\xi} = (\xi, \zeta)$. The technique is described in detail in.[36] The main idea is to define an inverse mapping governed by a pair of elliptic differential equations that, when solved with appropriate boundary conditions, gives $\mathbf{x}$, the coordinates of the computational nodes in the spatial domain. Thus, the coordinates ξ and ζ of the reference domain satisfy

$$\nabla \cdot (\mathbf{D} \cdot \nabla \boldsymbol{\xi}) = 0, \tag{23}$$

where $\nabla \equiv \partial/\partial \mathbf{x}$ denotes differentiation in physical space, and $\mathbf{D}$ is the diffusivity-like adjustable tensor that serves to control the gradients in coordinate potentials, and thereby the spacing between curves of constant ξ and constant ζ. With this technique, free boundaries are implicitly defined in the reference domain as boundaries where special boundary conditions are used. For example, the position of the free surfaces is calculated by imposing the kinematic condition, e.g. Eq.(9). The solid walls and synthetic inlet and outlet boundary planes are specified as functions of the coordinates and along them stretching functions are used to distribute conveniently the constant coordinate curves. Dynamic and static contact angles are imposed by replacing one of the elliptic mesh generation equation on the contact line node by Eq. (11); the other equation is replaced by the correspondig displacement restriction (see for example Eqs. (13) and (12)). The discrete versions of the mapping Eq. (23) are generally referred to as *mesh generation equations.*

3.2. Discretization by the finite element method

The weighted residual equations are obtained after multiplying the governing Eqs. (1), (2), (20), (22) and (23) by appropriate weighting functions associated with each degree of freedom ψ_i^c, ψ_i^m, ψ_i^ϕ, ψ_i^G and ψ_i^x, respectively, integrating over the unknown flow domain Ω (bounded by Γ), applying the divergence theorem to the diffusion terms (those with divergence) and mapping the integrals onto the known reference domain $\overline{\Omega}$ (bounded by $\overline{\Gamma}$). Details of this process are well known and were presented by Romero et al.[37] Here, this procedure is shown in detail only for the particle transport equation. After multiplying Eq. (20) by ψ_i^ϕ, integrate it over the spatial domain Ω, applying the divergence theorem to the appropriate term and mapping the integral to the reference domain, the weigthed residual becomes:

$$R_i^{\phi} \equiv \int_{\bar{\Omega}} \left[(\mathbf{v} \cdot \nabla \phi)\psi_i^{\phi} + (\bar{D}\nabla\phi \cdot \nabla\psi_i^{\phi}) + k_c a^2 \phi^2 (\nabla\dot{\gamma} \cdot \nabla\psi_i^{\phi}) \right] J d\bar{\Omega} - \int_{\bar{\Gamma}} \mathbf{n} \cdot \left[(\bar{D}\nabla\phi) + (k_c a^2 \phi^2 \nabla\dot{\gamma})\psi_i^{\phi} \right] (d\Gamma/d\bar{\Gamma}) d\bar{\Gamma} = 0, \qquad (24)$$

$J = \det(\mathbf{J}) = d\Omega/d\bar{\Omega}$ is the determinant of the Jacobian mapping and $\mathbf{n}$ is the outward unit normal vector to the boundary Γ. Thus, the last integral represents the diffusive particle flux on the boundaries of the flow domain. With the imposed boundary conditions, it is zero everywere to enforce the zero flux condition on solid surfaces (impermeability), free surfaces (no adsorption/desorption) and in the cross section of the film thickness (fully developed concentration profile).

Each independent variable is approximated with a linear combination of a finite number of basis functions, Thus, $\mathbf{v} \approx \sum_i \bar{\mathbf{v}}_i \varphi_i^m$, $\mathbf{x} \approx \sum_i \bar{\mathbf{x}}_i \varphi_i^{\mathbf{x}}$, $\phi \approx \sum_i \bar{\phi}_i \varphi_i^{\phi}$, $\mathbf{G} \approx \sum_i \bar{\mathbf{G}}_i \varphi_i^G$ and $p \approx \sum_i \bar{p}_i \varphi_i^c$. The quantities with overbar represent the coefficients of the expansions, i.e. the unknown of the discrete problem. The basis functions used to expand the independent variables are: Lagrangian bi-quadratic polynomials for velocity φ_i^m, position $\varphi_i^{\mathbf{x}}$ and concentration φ_i^{ϕ}, Lagrangian bi-linear polynomials for the interpolated velocity gradient φ_i^G and linear discontinuous polynomials for pressure φ_i^c. The Galerkin method is applied to the equations of momemtum, continuity, mesh generation and interpolated velocity gradient, i.e. $\psi_i^m = \varphi_i^m$, $\psi_i^c = \varphi_i^c$, $\psi_i^{\mathbf{x}} = \varphi_i^{\mathbf{x}}$, $\psi_i^{\mathbf{G}} = \varphi_i^{\mathbf{G}}$. Streamline Petrov-Galerkin is applied to the particle transport equation, i.e. $\psi_i^{\phi} = \varphi_i^{\phi} + h\mathbf{v} \cdot \nabla\varphi_i^{\phi}$. After replacing the interpolated variables in the corresponding weigthed residuals, the system of partial differential equations reduces to a simultaneous algebraic non-linear equations system for the coefficients of the basis functions of all fields.

A mesh with $1,312$ quadrilateral elements was used in all the results reported here. Increasing the number of elements by 50% in each direction did not significantly change the concentration and velocity profiles under the downstream die lip and coated film.

3.3. Solution of the non-linear system and validation

The system of equations was solved simultaneously for all variables using Newton's method. The entries of the Jacobian matrix **J** were evaluated numerically using a central finite difference scheme.[37] In each iteration the linearized equation system was factorized into unit lower **L** and upper **U** triangular matrices by a frontal solver. In order to assure the convergence of the Newton loop within 6 to 8 iterations, at each successive set of operating conditions (parameters), the initial guess was generated by a pseudo-arc-length continuation method.[38] The tolerance on the L2-norm of the residual vector and on the last Newton update of the solution was set to 10^{-6}.

To validate the model and the implementation, predictions were compared to the analytical solution of the fully developed, pressure driven particle suspension flow between parallel plates. As shown by Phillips et al.,[11] an analytical form for the velocity and concentration profiles can be obtained for the particular case of $k_c/k_\eta = 0.65$. The concentration profile is:

$$\phi = \frac{1}{1 + \frac{(1-\phi_w)y}{\phi_w}}\,, \tag{25}$$

where ϕ_w is the dimensionless particle concentration at the channel wall and y is the vertical coordinate in units of the channel half width H. On the symmetry line ($y = 0$), $\phi = 1$, because particles migrate towards the zero-shear rate region until the maximum packing concentration is reached. The velocity profile is then obtained by numerical integration (using trapezoidal rule) of the following expression:

$$u(y) = u^*(y)/u_{max} = 1 - \frac{dp}{dz}\frac{H^2}{2\eta_s u_{max}}\int_0^y \frac{y}{(1-\phi)^{-1.82}}dy, \tag{26}$$

where ϕ is given by Eq. (25).

The conditions of the problem used in the validation were: $L/H = 10$ and $\bar{\phi} = 0.59$. A parabolic velocity profile and a uniform concentration distribution were imposed in the inflow. In the outflow plane, we assumed a fully developed flow. Figure 2 shows the particle concentration field; as expected, the concentration near the wall, where the shear rate is high, is low and near the center line is high; that is, particles migrate from the high shear region towards the low shear region. Figure 3 depicts the particle concentration along both the centerline and channel wall. The results show that the channel length was long enough to reach the fully developed profiles at the exit plane. The particle distribution became fully developed (independent of x) at $x \approx 6H$. This entrance length is smaller than the one estimated by the scaling analysis presented by Nott and Brady.[18] With the set of parameters used in this validation case, the estimated entrance length should be $L_e \approx 40H$. We are not sure the reason for this difference. One possible explanation is that the scaling arguments used to estimate the entry length considers a shear-induced diffusion coefficient $D \approx \phi\dot{\gamma}a^2$, this corresponds

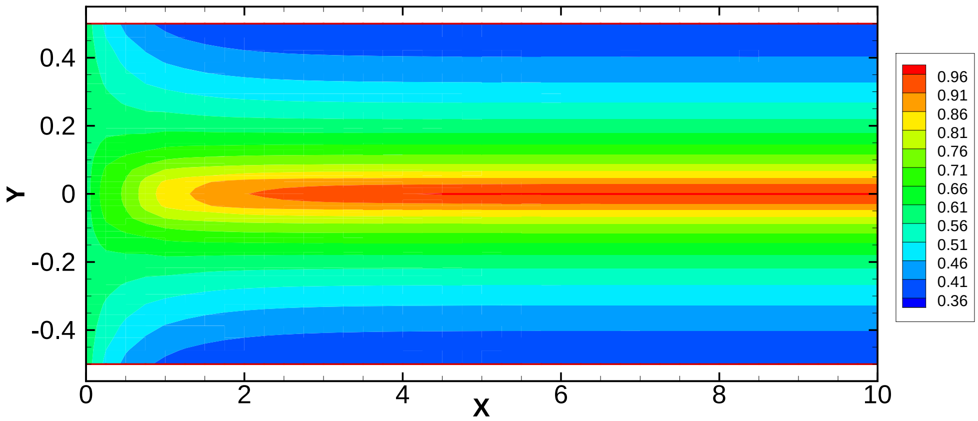

Figure 2: Particle concentration field in the supension inside a rectangular channel. On the left, a uniform concentration $\bar{\phi} = 0.59$ and a velocity profile given by Eq. (26) are imposed.

to the second term of eq.16. However, the total particle flux includes a second term, which accelerates the particle transport toward the center of the channel and should reduce the entrance length.

The computed velocity and concentration profiles at the outflow plane were compared to the fully-developed analytical solution in Figure 4. The agreement between the numerical prediction and exact solution is very good, showing a maximum error equal to 3.4% at the center line. This discrepancy is associated with the singularity at the symmetry line as explained below.

The diffusive flux model predicts particle migration towards regions where the deformation rate is low, that is, the symmetry line in this case. Actually, the simulations predicts values as high as $\phi = 1$, i.e. the maximum packing concentration. As $\phi \to 1$ the viscosity approaches infinity (see Eq. (4)), the Jacobian matrix becomes singular and the Newton's method fails. The

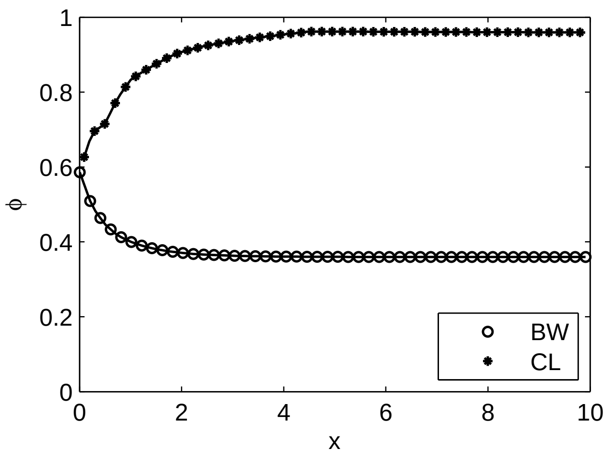

Figure 3: Particle concentration along the x-coordinate on the center line (CL) and bottom wall (BW) for the rectangular channel case shown in Figure 2.

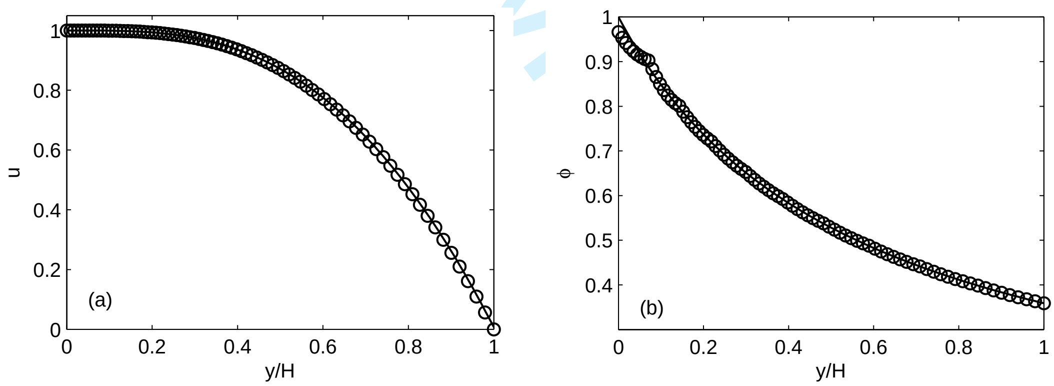

Figure 4: Comparison of the numerical results with the exact solution at the exit of the rectangular channel: a) velocity profile and b) concentration profile. In both cases, the continuous lines correspond with exact solution of the Eqs. (25) and (26).

singularity was avoided by using a strategy based in the concept of the *non-local stress* developed by Nott and Brady[18] and Miller and Morris.[39] At the particle scale, the continum hypothesis is not valid and the deformation rate is not correctly represented by $\underline{\underline{\dot{\gamma}}}$. As discused by Miller and Morris,[39] different approaches can be implemented to model this non-local stress but the main idea is that the shear rate at particle level is higher than the continuous representation and never goes exactly to zero. A small non-local shear rate value $\dot{\gamma}_{NL}$, which is a function of the particle size, is added to the local shear rate:

$$\dot{\gamma}_{NL} = a_s U_{loc}/l, \tag{27}$$

where $a_s = (a/l)^2$, l is the channel width and U_{loc} is the local fluid velocity (see Miller & Morris [41]). Thus, when Eq. (27) is added to the local deformation rate (Eq. (19)), the non-zero shear rate avoids the concentration reaching the maximum packing value.

4. Results

The flow under the downstream die lip is almost rectilinear and is well approximated by a superposition of Couette (substrate drag) and Poiseuille (pressure driven) flows. The pressure gradient is directly related to the imposed flow rate (film thickness).[40,41,42,43] For Newtonian flow, at a film thickness $t = t^*/H = 1/2$, the pressure gradient under the downstream die lip vanishes, the velocity profile is linear and the shear rate gradient is zero. At lower film thickness, an adverse pressure gradient occurs to counter act the drag from the substrate. At $t = 1/3$, the shear rate at the die surface vanishes. At even lower flow rate, flow reversal occurs near the die surface and a recirculation appears. Since particle migration is driven by shear rate gradient, the final particle distribution in the coated layer should be strongly affected by the imposed film thickness.

In this work, the flow topology and particle distribution are analyzed at three different values of the film thickness, e.g. $t = 0.5$, $t = 0.37$ and $t = 0.14$. The flow of the particle suspension is compared to the equivalent case at which particle migration is not taken into account and the viscosity of the liquid is constant throughout the flow (equal the viscosity of the suspension at the average bulk particle concentration).

Table 1 shows the values of the dimensional parameters used in this study. The corresponding capillary number is $Ca = 0.1$. The values of the coefficients of the diffusive flux model (k_c and k_η) were in the same order of the experimental values determined by Phillips et al.[11]

4.1. Flow state at $t/H_0 = 0.5$

As was mentioned before, the pressure gradient under the die lip vanishes for Newtonian flow at $t/H_0 = 0.5$, and the flow is well approximated by a pure Couette flow. This imply that the shear rate is almost constant in this region. Figure 5-a shows the particle concentration field for this condition. In the feed slot, particles migrate towards the symmetry plane, from the high shear region near the wall towards the low shear region in the symmetry plane. At the exit of the feed slot, the concentration at the center of the channel is close to the maximum packing concentration.

Detail of the particle concentration field in the upstream part of the coating bead is presented in Figure 5-b. The particle concentration near

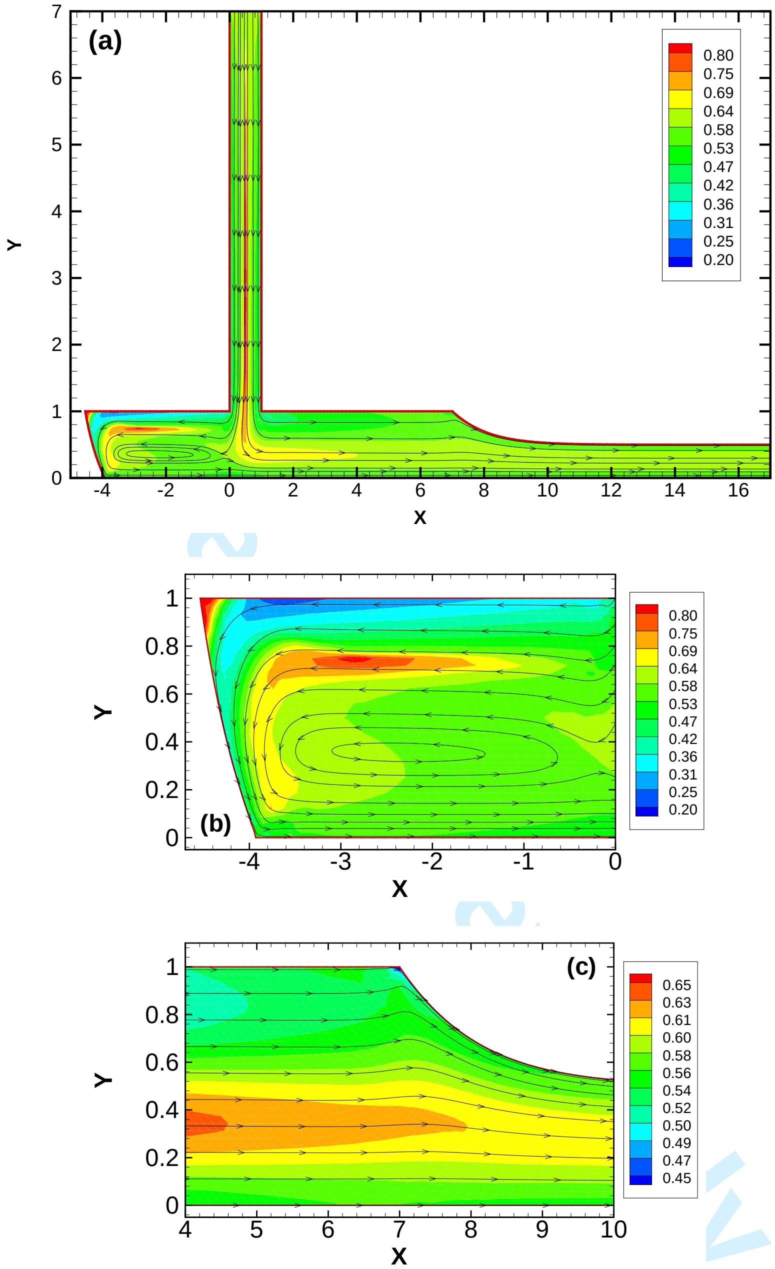

Figure 5: a) Particle concentration field and selected streamtraces in the domain, for the parameters listed in Table 1. b) Zoom on the upstream slot coating region, showing the region of high particle concentration near the upstream static contact line. c) Zoom of the downstream slot coating region.

V_s	0.1 $[m/s]$
P_{vac}	-3.7 $[kPa]$
σ	0.06 $[N/s]$
η_s	0.06 $[Pa\,s]$
a	4 $[\mu m]$
H_s	10^{-4} $[m]$
H_0	10^{-4} $[m]$
$\bar{\phi}$	0.59
k_c	0.816
k_η	1.22

Table 1: Values of the parameters used in the simulation with $t = 0.5$

the die lip is low, because particles migrate from this high shear rate zone close to the die surface towards a low shear rate region near a layer where the deformation rate almost vanishes ($y \sim 0.7$).

The correct description of the effect of vacuum pressure on the upstream meniscus position needs to take into account that the viscosity of the liquid attached to the die lip is lower than the viscosity at the average particle concentration. Figure 6 presents the pressure along the substrate in the upstream bead for the flow of a particle suspension and the equivalent Newtonian flow that does not take particle migration into account. In the later, the liquid viscosity was set at the value of the average concentration, $\bar{\phi} = 0.59$, and was constant throughout the flow; e.g. $\eta_r(\bar{\phi}) = 5.3$. The lower viscosity of the liquid attached to the substrate and die lip reduces the necessary ad-

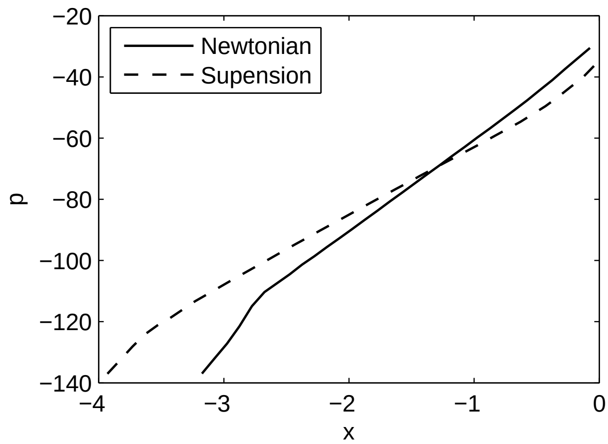

Figure 6: Pressure on the moving substrate in the upstream region, for the conditions of Table 1 (Suspension) and the same parameters but without particle migration (Newtonian).

verse pressure gradient to counteract the drag by the substrate. Therefore, for a fixed vacuum pressure, the meniscus is located further away from the feed slot. Although not explored here, the lower and upper vacuum pressure operability limits in slot coating window (see Carvalho and Keshghi[41]) are modified when particle transport is taken into consideration in the model.

Figure 5 shows that for these conditions, the high particle concentration near the center of the feed slot is convected through the downstream coating bead with weak particle diffusion, leading to high particle concentration in a layer located at $y \sim 0.4$. For $t = 0.5$, the velocity profile under the downstream die lip is close to a linear profile (Couette flow), as show in Figure 7-a. The shear rate is almost constant and particle migration is only driven by viscosity gradient, that forces particle to diffuse from high viscosity (high concentration) regions to lower viscosity (low concentration) regions.

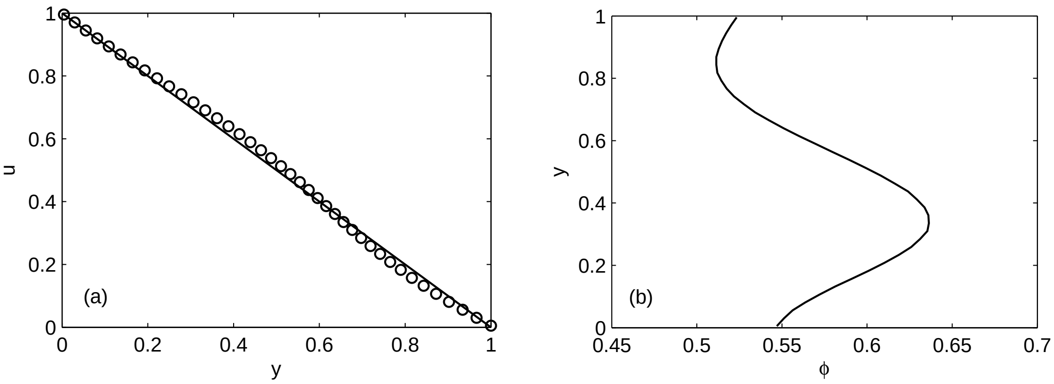

Figure 7: Velocity (a) and concentration (b) profiles at $x \sim 4$ for the case with $t = 0.5$ (Figure 5). The theoretical profile of a Coutte flow is also included for comparison (continuous line in frame (a)).

However, at the conditions analyzed, this effect is weak and the concentration profile at $x \sim 4$ (middle of downstream lip) shows a layer of higher particle concentration ($\phi \sim 0.65$) at $y \sim 0.4$.

The concentration field near the downstream free surface is shown in Figure 5-c. Close to the static contact line, the deformation rate is high leading to a region of low particle concentration ($\phi \sim 0.4$). The layer of high particle concentration remains in the final film, as shown in Figure 8. The concentration at the substrate and at the free surface ($\phi \approx 0.56$) are lower than the average particle concentration $\bar{\phi} = 0.59$ and there is a layer of higher particle concentration ($\phi \approx 0.61$) located approximately in the middle of the coated layer.

4.2. Flow state at $t/H_0 \sim 1/3$

As discussed before, at $t/H_0 = 1/3$ and constant viscosity, the adverse pressure gradient is such that the deformation rate vanishes at the down-

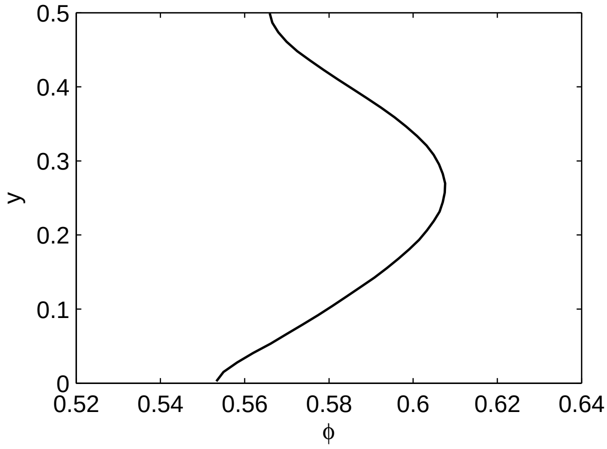

Figure 8: Concentration profile along the cross section of the coated film ($x = 17$).

stream slot die wall. According to the diffusive flux model, particles will migrate towards this region. The non-uniform shear rate flow completely changes the particle concentration field in the downstream coating bead and on the final coated film, when compared to the case at $t/H_0 = 0.5$.

In this section, the flow field at $t/H_0 = 0.37$ is presented. At this condition, the zero shear rate is not located exactly at the wall, but very close it. The flow (represented by streamtraces) and particle concentration field are presented in Figure 9-a. The upstream flow and particle distribution pattern (Figure 9-b) are similar to that presented in Figure 5-b (at $t/H_0 = 1/2$). By contrast, the downstream behavior presented in Figure 9-c is quite different. A high particle concentration region is formed close to the dip lip surface. The velocity and concentration profile across the coating gap at $x \sim 4$ is shown in Figure 10. The low shear rate close to the die wall and corresponding high particle concentration is clearly observed. The high particle concentration layer is convected to the top of the coated film. The concentration profile across the thickness of the coated layer is shown in Figure 11. Now, the particle concentration on the free surface ($\phi \sim 0.62$) is higher than the average concentration, $\bar{\phi} = 0.59$. This can have a tremendous effect on the drying process and particle structure formation.

4.3. Flow state at $t/H_0 < 1/3$

At film thickness lower than 1/3 of the coating gap, i.e. $t/H_0 < 1/3$, the adverse pressure gradient under the downstream die lip is strong enough that a recirculation is formed. This session presents results at very thin films, $t = 0.14H_0$, with $k_c = 0.34$ and $k_\eta = 0.51$. The coefficients of the diffusive flux model were changed because it was not possible to obtain converged solution for the values of Table 1. We infer that the convergence problems were associated to the high concentration gradients associated to particle accumulated inside the recirculation, which are very steep to be capture by our mesh refinement.

The flow and particle concentration field are shown in Fig. 12. The recirculation under the die lip has a strong effect on the particle distribution in the coating bead, because a region of high particle concentration is formed inside the recirculation. The backflow creates a layer of maximum negative velocity and vanishing shear rate towards which particles migrate. This high particle concentration inside a vortex may promote particle aggregation which is usually undesired. Because of the large recirculation, all the liquid comming from the feed slot flows back to the upstream bead before being dragged by the substrate. The high particle concentration layer at the center of the feed is re-distributed in this process and, due to particle migration from the substrate, a layer with higher concentration is created close the flow separating

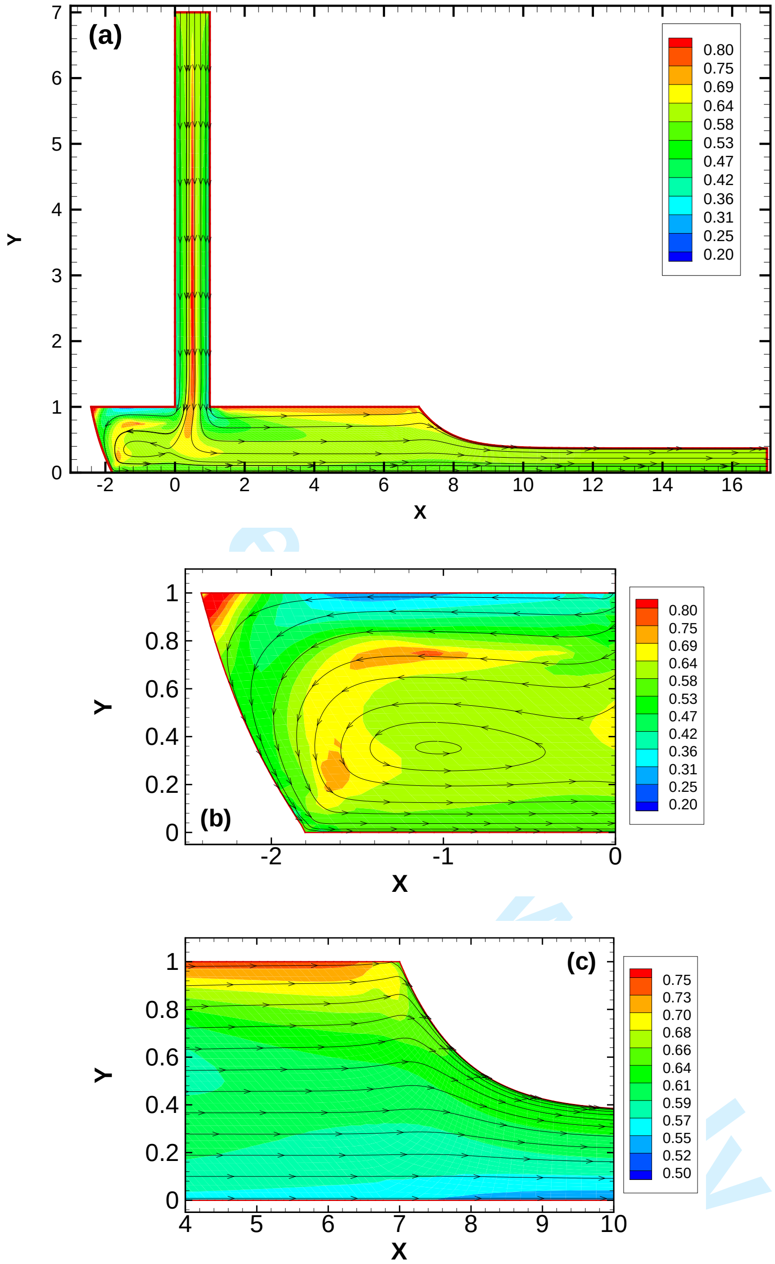

Figure 9: As in Figure 5 but for $t = 0.37$.

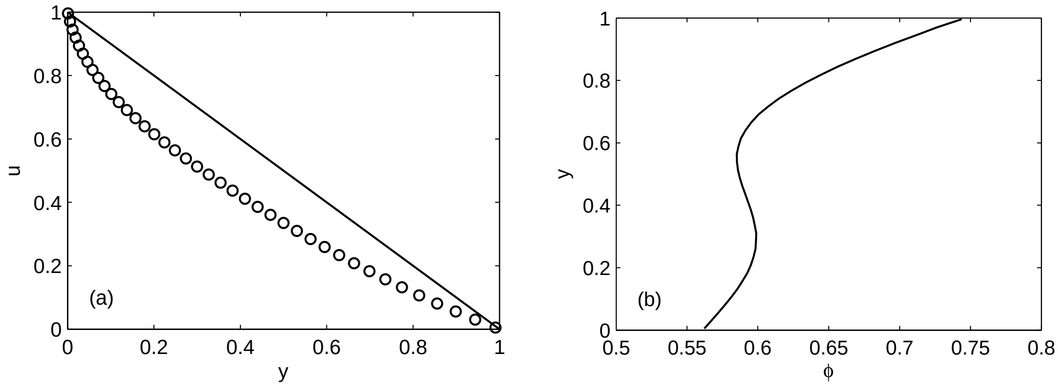

Figure 10: Velocity (a) and concentration (b) profiles at $x \sim 4$ for the case with $t = 0.37$ (Figure 9). The theoretical profile of a Coutte flow is also included for comparison (continuous line in frame (a)).

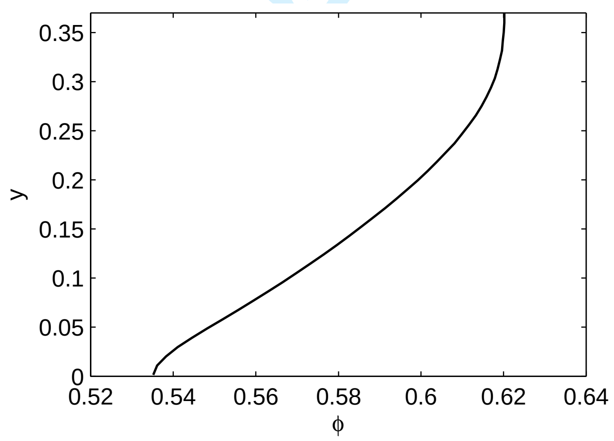

Figure 11: Concentration profile along the cross section of the coated film ($x = 17$), for $t = 0.37$.

streamline that terminates at the meniscus stagnation point. This explains the shape of the profile across the coated film as presented in Fig.13. The particle distribution is similar to the one obtained at $t = 0.37$ with the high concentration at the top of the film ($\phi \sim 0.62$) and low ($\phi \sim 0.54$) at the substrate.

5. Final Remarks

Slot coating flow of non-colloidal particle suspensions was studied to determine the effect of operating conditions on the particle distribution in the coating bead and deposited liquid layer. The flow was described by the mass and momentum conservation equations coupled with a particle transport equation based on the diffusive flux model proposed by Phillips et al.[11] The viscosity was considered a function of the local particle concentration and independent of the local shear rate. The problem was discretized using the finite element method and the unknown domain and free surface was mapped with an elliptic mesh generation technique. The resulting set of algebraic nonlinear equations was solved using the Newtons method.

The results show that the particle distribution in the coating bead is non-uniform. The complex flow field leads to shear induced particle transport. Since the deformation rate field is strongly dependent on the imposed flow rate (wet thickness), the particle distribution in the flow and consequently in the coated layer drastically changes as the film thickness varies. When the film thickness is 1/2 of the coating gap, the shear under the downstream die lip is almost constant and the high particle concentration region formed in the center of the feed slot is convected, leading to a high particle concentration

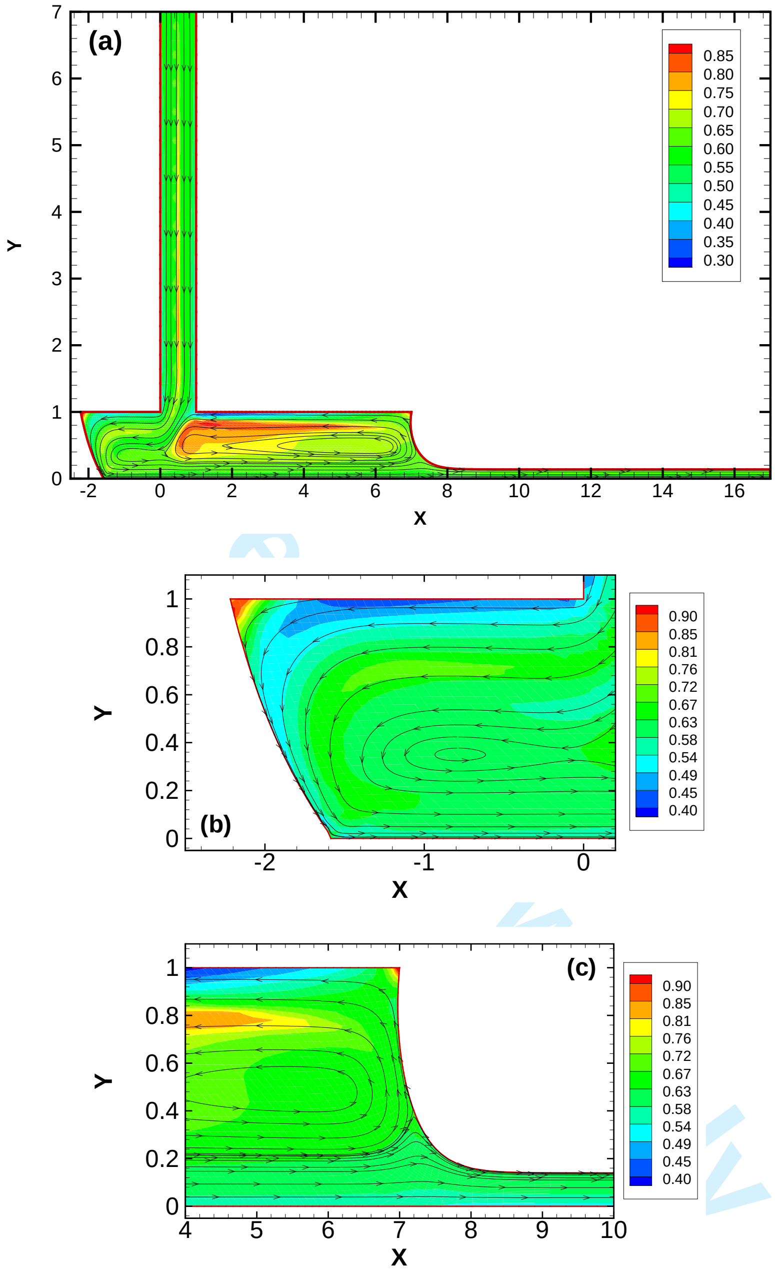

Figure 12: As in Figure 5 but for $t = 0.14$.

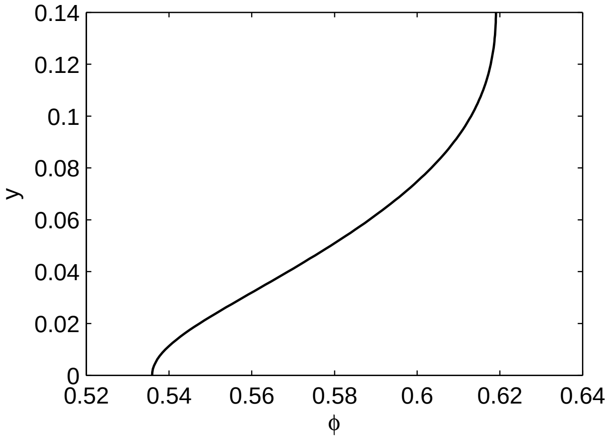

Figure 13: Concentration profile along the cross section of the coated film ($x = 17$), for $t = 0.14$.

layer in the middle of the coated film. At a film thickness close to 1/3 of the coating gap, particles are transported towards the zero-shear region close to the die lip, leading to high particle concentration in the die surface and on the surface of the coated layer. The high concentration in the die lip may have a strong effect on particle agglomeration and streak formation that ultimately leads to coating defects. At even lower flow rates, particles accumulate inside the flow recirculation, which also may lead to undesirable agglomeration and coating defects.

Although experimental results on particle distribution in the liquid layer deposited using slot coating is not available, it is clear that is has a strong effect on the flow and drying processes, and microstructure formation. The effect of particles in the coating liquid on the operability limits of the process has been reported.[44]

The results presented here show that process conditions (wet thickness) can be used to obtain the desired particle distribution. The two-dimensional, steady-state flows can be used as base state for stability analysis, to determine the conditions at which the flow ceases to be two-dimensional and steady, which are usually associated with process limits.[41]

A natural extension of the model is to consider particles that are not neutrally buoyant and the surface tension as a function of local particle concentration.[45] The present results shown high concentration gradients at the downstream interface that may generate strong Marangoni stresses if the surface tension varies locally with the particle concentration. This tangential stresses could have a deep impact on the flow field,[46] the interface shape and, consequently on the operability window of the process.

Acknowledgments

The authors would like to thank to the following institutions for financial support: *Fundação de Amparo à Pesquisa do Estado do Rio de Janeiro* (FAPERJ), *Conselho Nacional de Desenvolvimento Científico e Tecnológico* (CNPq-Brazil), *Consejo Nacional de Investigaciones Científicas y Técnicas* (CONICET-Argentina) and the program *Industrial Partnership for Research in Interfacial and Material Engineering* (IPRIME) of the University of Minnesota.

References

[1] Cardinal CM, Jung YD, Ahn KH, Francis LF. Drying regime maps for particulate coatings. *AIChE Journal.* 2010;56(11):2769–2780.

[2] Chang CY, Powell RL. Hydrodynamic transport properties of concentrated suspensions. *AIChE Journal*. 2002;48:2475–2480.

[3] Stickel JJ, Powell RL. Fluid mechanics and rheology of dense suspensions. *Annual Review of Fluid Mechanics*. 2005;37:129–449.

[4] Santamaria-Holek I, Mendoza CI. The rheology of hard sphere suspensions at arbitrary volume fractions: an improved differential viscosity model. *Journal of Chemical Physics*. 2009;130(044904):1–7.

[5] Shewan HM, Stokes JR. Analytically predicting the viscosity of hard sphere suspensions from the particle size distribution. *Journal of Non-Newtonian Fluid Mechanics*. 2015;222:79–81.

[6] Karnis A, Goldsmith AL, Mason SG. The kinetics of flowing dispersions: concentrated suspensions of rigid particles. *Journal of Non-Newtonian Fluid Mechanics*. 1966;22:531–553.

[7] Gadala-Maria F, Acrivos A. Shear-induced structure in a con-centrated suspension of solid spheres. *Journal of Rheology*. 1980;24:799–814.

[8] Leighton D, Acrivos A. Measurement of shear-induced self-diffusion in concentrated suspensions of spheres. *J Fluid Mechanics*. 1987;177:109–131.

[9] Graham AL, Altobelli SA. NMR imaging of shear-induced diffusion and structure in concentrated suspensions. *Journal of Rheology*. 1991; 35:191–201.

[10] Altobelli SA, Givler RC. Velocity and concentration measure-ments of suspensions by nuclear magnetic resonance imaging. *Journal of Rheology*. 1991;35:721–734.

[11] Phillips RJ, Armstrong RC, Brown RA, Graham AL, Abbott JR. A constitutive equation for concentrated suspensions that accounts for shear-induced particle migration. *Physics of Fluids A: Fluid Dynamics*. 1992; 4(1):30–40.

[12] Chow AW, Sinton SW, Iwamiya JH, Stephens TS. Shear-induced migration in couette and parallel-plate viscometers: NMR imaging and stress measurements. *Physics of Fluids*. 1994;6:2561–2576.

[13] Hampton RE, Mammoli AA, Graham AL, Tetlow N, Altobelli SA. Migration of particles undergoing pressure-driven flow in a circular conduit. *Journal of Rheology*. 1997;41:621–640.

[14] Subia SR, Ingber MS, Mondy LA, Altobelli SA. Modelling of concentrated suspensions using a continuum constitutive equation. *Journal of Fluid Mechanics*. 1998;373:193–219.

[15] Krishnan GP, Beimfohr S, Leighton D. Shear-induced radial segregation in bidisperse suspensions. *Journal of Fluid Mechanics*. 1996;321:371–393.

[16] Kim JM, Lee SG, Kim C. Numerical simulations of particle migration in suspension flows: frame-invariant formulation of curvature-induced migration. *Journal of Non-Newtonian Fluid Mechanics*. 2008;150:172–176.

[17] Tetlow N, Graham AL, Ingber MS, Rubia SR, Mondy LA, Altobelli SA. Particle migration in a Couette apparatus: experiment and modeling. *Journal of Rheology*. 1998;42:307–327.

[18] Nott PR, Brady JF. Pressure-driven flow of suspensions: simulation and theory. *Journal of Fluid Mechanics*. 1994;275:157199.

[19] Ritz JB, Bertrand F, Thibault F, Tanguy PA. Shear-induced particle migration in a short-dwell coater. *Chemical Engineering Science*. 2000; 55:4857–4867.

[20] Rao RR, Mondy LA, Altobelli SA. Instabilities during batch sedimentation in geometries containing obstacles: A numerical and experimental study. *International Journal of for Numerical Methods in Fluids*. 2007; 55:723–735.

[21] Ahmed GMY, Singh A. Numerical simulation of particle migration in asymmetric bifurcation channel. *Journal of Non-Newtonian Fluid Mechanics*. 2011;166:42–51.

[22] Chong JS, Christiansen EB, Baer AD. Rheology of concentrated suspensions. *Journal of Applied Polymer Science*. 1971;15(8):2007–2021.

[23] Metzner AB. Rheology of Suspensions in Polymeric Liquids. *Journal of Rheology*. 1985;29(6):739–775.

[24] Mewis J, Frith WJ, Strivens TA, Russel WB. The rheology of suspensions containing polymerically stabilized particles. *AIChE Journal*. 1989;35(3):415–422.

[25] Furusawa T, Smith JM. Fluid-Particle and Intraparticle Mass Transport Rates in Slurries. *Industrial and Engineering Chemistry Fundamentals*. 1973;12(2):197–203.

[26] Lenoble M, Snabre P, Pouligny B. The flow of a very concentrated slurry in a parallel-plate device: Influence of gravity. *Physics of Fluids*. 2005; 17(7):073303.

[27] Timberlake BD, Morris JF. Concentration band dynamics in free-surface Couette flow of a suspension. *Physics of Fluids*. 2002;14(5):1580–1589.

[28] Furbank RJ, Morris JF. An experimental study of particle effects on drop formation. *Physics of Fluids*. 2004;16(5):1777–1790.

[29] Apostolou K, Hrymak AN. Discrete element simulation of liquid-particle flows. *Computers & Chemical Engineering*. 2008;32(4-5):841–856.

[30] Min KH, Kim C. Simulation of particle migration in free-surface flows. *AIChE Journal*. 2010;56(10):2539–2550.

[31] Krieger IM. Rheology of monodispersed latices. *Advances in Colloid and Interface Science*. 1972;3(2):111–136.

[32] Huh C, Scriven LE. Hydrodynamic model of steady movement of a solid/liquid/fluid contact line. *J Colloid Interface Sci*. 1971;35:85–101.

[33] Bird RB, Armstrong RC, Hassager O. *Dynamics of polymeric liquids: Fluid mechanics*, vol. 1. John Wiley & Sons, New York, USA. 1977.

[34] Szadi M, Salmon T, Liu A, Bornside D, Armstrong R. New mixed finite element method for viscoelastic flows governed by differential constitutive equations. *Journal of Non-Newtonian Fluid Mechanics*. 1995; 59:215–243.

[35] Pasquali M, Scriven LE. Free surface flows of polymer solutions with models based on the conformation tensor. *Journal of Non-Newtonian Fluid Mechanics*. 2002;108:363–409.

[36] Christodoulou KN, Kistler SF, Schunk PR. *Advances in computational methods for free-surface flows*. Chapman Hall, London, UK. 1997.

[37] Romero OJ, Carvalho MS, Scriven LE. Slot Coating of Mildly Viscoelastic Liquids. *Journal of Non-Newtonian Fluid Mechanics*. 2006;138:6375.

[38] Chang TFC, Keller HB. Arc-length continuation and multi-grid techniques for nonlinear elliptic eigenvalue problems. *SIAM J ScI Stat Comput*. 1982;3(2):173194.

[39] Miller RM, Morris JF. Normal stress-driven migration and axial development in pressure-driven flow of concentrated suspensions. *Journal of Non-Newtonian Fluid Mechanics*. 2006;135(2-3):149165.

[40] Sartor L. Slot Coating: Fluid Mechanics and Die Design. PhD Thesis, University of Minnesotta. 1999.

[41] Carvalho MS, Kheshgi HS. Low-flow limit in slot coating: Theory and experiments. *AIChE Journal*. 2000;46(10):1907–1917.

[42] Lee AG, Shaqfeh ESG, Khomani B. A study of viscoelastic free surface flows by the finite element method: Hele-Shaw and slot coating flows. *Journal of Non-Newtonian Fluid Mechanics*. 2002;108(1-3):327362.

[43] Romero O, Suszynski W, Scriven L, Carvalho M. Low-flow limit in slot coating of dilute solutions of high molecular weight polymer. *Journal of Non-Newtonian Fluid Mechanics*. 2004;118(23):137 – 156.

[44] Chu WB, Yang JW, Wang YC, Liu TJ, Tiu C, Guo J. The effect of inorganic particles on slot die coating of poly(vinyl alcohol) solutions. *Journal of Colloid and Interface Science*. 2006;297(1):215–225.

[45] Binks BP. Particles as surfactant: similarities and differences. *Current Opinion in Colloid & Interface Science*. 2002;7:21 – 41.

[46] Campana DM, Ubal S, Giavedoni MD, Saita FA. Numerical prediction of the film thickening due to surfactants in the Landau−Levich problem. *Phys Fluids*. 2010;22:032103.

Slot coating flows of non-colloidal particle suspensions

L. D. Valdez Silva[b], D. M. Campana[a], M. S. Carvalho[b,*]

[a] *Instituto de Desarrollo Tecnológico para la Industria Química, CONICET, Güemes 3450, Santa Fe, 3000, República Argentina*
[b] *Department of Mechanical Engineering, Pontificia Universidade Catolica do Rio de Janeiro, Rua Marques de Sao Vicente 225, Gavea, Rio de Janeiro, RJ, 22453-900, Brazil*

Abstract

Slot coating is used in the manufacturing of functional films, which rely on specific particle microstructure to achieve the desired performance. Final structure on the coated film is strongly dependent on the suspension flow during the deposition of the coating liquid and on the subsequent drying process. Fundamental understanding on how particles are distributed in the coated layer enables optimization of the process and quality of the produced films.

The complex coating flow leads to shear-induced particle migration and non-uniform particle distribution. We study slot coating flow of non-colloidal suspensions by solving the mass and momentum conservation equations coupled with a particle transport equation using the Galerkin/Finite element method. The results show that particle distribution in the coating bead and in the coated layer is non-uniform and is strongly dependent on the imposed flow rate (wet thickness).

Keywords:

*Corresponding author. Email address: msc@puc-rio.br

Preprint submitted to AIChE Journal *May 16, 2016*

free surface flow, slot coating, particle suspension

1. Introduction

Many coated products, such as anti-reflection, hydrophobic films and flexible electrodes, rely on a designed microstructure in order to achieve the desired functionality. One way of mass producing functional coated films is by depositing a particle suspension onto a moving substrate and subsequently drying the liquid to form the final solid film. The final microstructure of the coated layer is directly affected by the suspension flow during the coating and drying processes, due to particle migration effects. Cardinal et al.[1] have shown how the relative strength of liquid evaporation, particle diffusion and sedimentation affect the particle distribution on the coated film during drying. A 1-D particle conservation equation was used to describe the particle concentration evolution during drying by taking into account for the aforementioned effects, while cryo-electron microscopy images were used to validate the predicted drying map. However, the model assumes that the particle concentration is uniform through the thickness of the film in the initial stages of drying. This may not be the case when the liquid film is deposited on the substrate by slot coating process, for example, where high shear rate gradient are developed in the coating bead.

If the suspended particles are large enough, Brownian motion, van der Walls and electrical double layer forces between particles can be neglected and the resulting liquid is a non-colloidal suspension. In this condition, the suspension viscosity becomes a function of the particle volume fraction only.[2,3,4,5] When this suspension is set in non-uniform flow (as those mostly encountered in coating processes), particles are transported by convection, sedimentation/buoyancy and shear rate and viscosity gradient driven diffusion. The last two mechanisms are frequently called *shear-induced* particle migration. This behavior was described, for example, in the suspension flows inside cylindrical tubes[6] and in the Coutte flow between concentric cylinders.[7] The main observation was that particles migrate from regions with higher to lower shear rate. Later, Leighton and Acrivos[8] developed a rational explanation for these mechanisms based on the frequency of the inter-particle collisions and the effective viscosity of the suspension, both being functions of the non-uniform local particle volume fraction. This phenomena has been confirmed experimentally in different situations.[9,10]

Based on the work of Leighton and Acrivos,[8] Phillips et al.[11] proposed a convective-diffusion equation that describes the particle concentration variation in laminar flows. This approach was called diffusive flux model and depends on two diffusion parameters, which they considered as constants to be fitted using experimental results. By considering the fluid as Newtonian, but with the viscosity being function of the local particle concentration, Phillips et al.[11] solved the particle transport equation coupled with the momentum conservation for two flow configurations: Poiseuille pressure driven flow in a circular tube and Couette flow between rotating cylinders. The diffusive flux model was also successfully used in different analyses.[12,13,14] However, the model cannot correctly predict the radial particle migration of some viscometric flows and different improvements and corrections have been proposed. For example, Krishnan et al.[15] suggested that the curvature of streamlines also contributes to the radial particle migration. More recently, Kim et al.[16] developed a model to take into account this curvature-induced particle flux. Tetlow et al.[17] also suggested that the diffusion parameters of the model should depends on the local particle concentration.

Another approach to study particle migration in flows of concentrated suspensions is the Suspension Balance Model, which was first proposed by Nott and Brady.[18] Its physical concept is that the migration phenomenon arises in order to balance a non-homogeneous normal stress that exists due to the presence of the particles. The particle flux is directly proportional to the divergence of the particle stress tensor (i.e., an additional stress in the fluid phase stress tensor). They show that in a simple shear flow, the suspension balance model leads to a diffusion equation of the same form as the one obtained with the diffusive flux model.

Despite its limitations, the original diffusive flux model[11] is relatively simple to implement in computational codes and has been used to study more complex flows. For example, Ritz et al.[19] used the model to calculate the particle distribution inside a short-dwell coater, Rao et al.[20] to describe instabilities on bath sedimentation problems and Ahmed and Singh[21] implemented the model to calculate the particle distribution downstream a bifurcation channel. We apply the model to study steady slot coating flow of particle suspensions.

Particle migration has tremendous impact on rheological measurements of particle suspensions [22, 23, 24] and on different process flows of slurries [25, 26]. The effect of particles is also even more pronounced when the flow has free surfaces, as discussed by Timberlake and Morris[27] and Furbank and Morris[28] on the drop formation and pinch-off of pendant/ejected drops. The non-uniform particle distribution that leads to viscosity variation within the flow triggers different flow instabilities.

Despite its fundamental importance in fluid mechanics and industrial applications, analysis of coating flows of particle suspension that takes into account particle migration mechanisms is still rare in the literature. One usual approach is to consider the liquid as a Newtonian or a shear-thinning fluid using the viscosity (or viscosity curve) evaluated at the average particle concentration. However, the complex flow in the coating bead may lead to particle migration and non uniform particle distribution downstream of the film formation region. An alternative approach is to study particle distribution in the flow assuming that the flow is not affected by the particles.[29]

Up to our knowledge, there is no experimental measurements of particle distribution in the liquid coated film. Theoretical and numerical analyses are also rare. The only exception for a two-way coupling between flow and particle transport is the work of Min and Kim[30] who studied numerically, using the finite volume method, the effect of particle migration in two free surface flows. Using the diffusive flux model,[11] they first computed the flow field and particle distribution in a planar liquid jet ejected from two parallel plates, obtaining results for different particle sizes, mean particle concentrations and Reynolds numbers. They also solved the flow for a slot coating configuration, but due to convergence problems in the numerical technique used, the range of operation parameters explored was limited.

The aim of this work is to study slot coating flow of non-colloidal particle suspension for flow conditions typically encountered in industrial applications. The steady-state, two-dimensional momentum, mass conservation and the particle transport equations for the free boundary problem were solved in a fully coupled scheme using the Galerkin/Finite element method. The effect of particle migration on the steady flow states is the first step towards a fundamental understanding on how the presence of particles suspended in the coating liquid can affect the operating window of the process, i.e. the conditions at which the flow becomes transient or three-dimensional. The steady-state solutions presented here can be used as base state for stability analysis of the flow.

The paper is organized as follow: section 2 presents the governing equations and boundary conditions for the fluid flow problem (section 2.1) and particles transport (section 2.2); the numerical technique is explained in sections 3.1 and 3.2, while validation results are discussed in section 3.3. Finally, section 4 presents the new results and section 5 is devoted for the final remarks.

2. Mathematical formulation

In slot coating process, the liquid is pumped to a coating die in which an elongated chamber distributes it across the width of a narrow slot. Exiting the slot, the liquid fills (wholly or partially) the gap H_0 between the adjacent die lips and the substrate translating rapidly past them at a speed V_s. The liquid in the gap, bounded upstream and downstream by gas-liquid interfaces, or menisci, forms the coating bead, as shown in Fig. 1. In order to sustain the coating bead at higher substrate speeds and smaller wet thickness, the gas pressure at the upstream meniscus is made lower than ambient, i.e. a slight vacuum p_{vac} is applied to the upstream meniscus. The

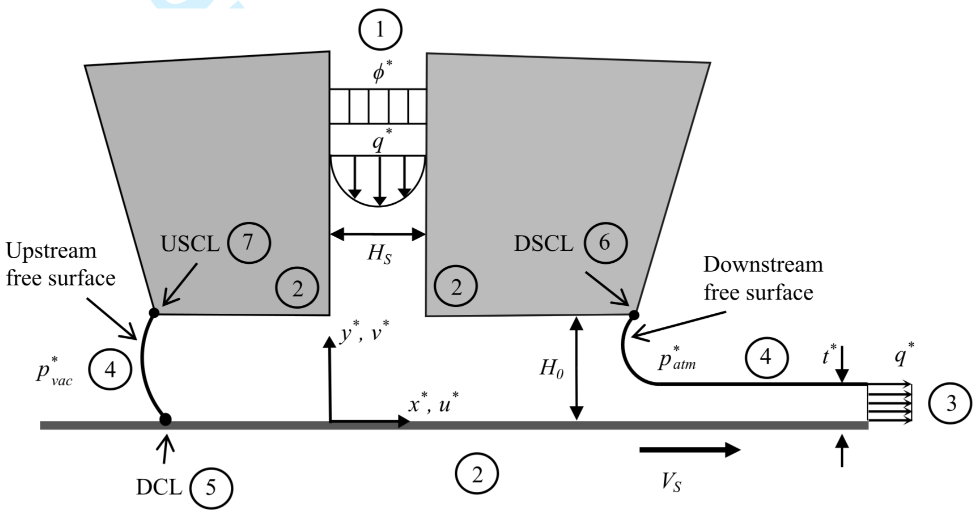

Figure 1: Sketch of the slot coating head, moving substrate and coated film. The boundaries are denoted by number according the imposed boundary conditions.

upstream meniscus is bounded by the upstream contact line (USCL in Fig.1) and the dynamic contact line (DCL) where the liquid wets the moving substrate. The downstream meniscus starts at the downstream static contact line (DSCL in Fig.1). Slot coating belongs to a class of coating methods known as *pre-metered coating*: the thickness t of the coated layer is set by the flow rate fed to the coating die q and the speed of the moving substrate, and is independent of the other process variables, i.e. $t = q/V_s$.

2.1. Governing equations for fluid flow

In this work we neglect both the inertial and gravitational effects based on the fact that the flow dimension is very small, e.g. $H_0 \approx 100\mu$m. Thus, the velocity $\mathbf{v} = u\mathbf{i} + v\mathbf{j}$ and pressure p fields of the two-dimensional and steady Stokes flow are governed by the continuity and momentum equations for incompressible liquid:

$$\nabla \cdot \mathbf{v} = 0 \tag{1}$$

$$\nabla \cdot \mathbf{T} = \nabla \cdot [-p\mathbf{I} + \tau] = 0 \tag{2}$$

The parameter η_s represents the constant dynamic viscosity of the solvent. Because we are considering non-colloidal suspensions, the viscous stress τ is taken to be a linear function of the rate-of-strain tensor. The viscosity of the suspension is only a function of the local particle concentration ϕ and does not vary with the deformation rate:

$$\begin{gathered} \tau = \eta(\phi)\underline{\underline{\dot{\gamma}}} \\ \underline{\underline{\dot{\gamma}}} = \nabla \mathbf{v} + \nabla \mathbf{v}^T \end{gathered} \tag{3}$$

The relative viscosity of the suspension is defined as $\eta_r(\phi) = \eta(\phi)/\eta_s$. According to the empirical observation of Krieger,[31] the relative viscosity of a non-colloidal suspension (high Péclet number, $Pe \gg 1$) is well approximated by

$$\eta_r = (1 - \phi^*)^{-1.82}, \tag{4}$$

where $\phi^* = \phi/\phi_m$ is the relative particle volume fraction, being ϕ_m the *maximum packing concentration.*

The relative viscosity of the suspension η_r approaches infinity as the particle concentration approaches the maximum packing concentration, which for rigid spheres is $\phi_m \sim 0.68$. Although Eq.(4) was originally proposed for suspensions with $0.01 < \phi < 0.5$, we follow the same approach of Phillips et al.[11] and consider that it is valid for $0.01 < \phi < 0.68$.

The following boundary conditions are applied to the momentum conservation equation; the boundaries are identified by corresponding numbers in Fig. 1:

1. At the inflow of the feed slot, the flow is fully developed and the velocity profile given by

$$\mathbf{v} = -6V_s t \left[(x/H_s) - (x/H_s)^2 \right] \mathbf{j}, \tag{5}$$

   where V_s is the substrate speed, t is the film thickness and H_s the width of the feed channel.

2. Along the solid surfaces, no-slip and no penetration conditions are applied

$$\mathbf{v} = 0, \text{ along feed channel and slot die walls}$$
$$\mathbf{v} = \mathbf{i}, \text{ along substrate} \tag{6}$$

3. Along the outflow plane, the flow is assumed to be fully developed and the pressure is set to the ambient pressure p_{amb}:

$$\mathbf{n} \cdot \nabla \mathbf{v} = 0$$
$$p = p_{amb} \tag{7}$$

In this work, the constant ambient pressure is arbitrary set as $p_{amb} = 0$.

4. Along the free surfaces, the kinematic condition and force balance are applied:

$$\mathbf{n} \cdot \mathbf{T} = (\sigma\kappa - p_{amb})\,\mathbf{n} \tag{8}$$

$$\mathbf{n} \cdot \mathbf{v} = 0, \tag{9}$$

where $p_{amb} = 0$ and $p_{amb} = p_{vac}$ on the downstream and upstream free surfaces, respectively. In addition, $\kappa = -\nabla_s \cdot \mathbf{n}$ is the interface curvature, $\nabla_s = (\nabla - \mathbf{nn})$ the surface gradient operator, $\mathbf{n}$ the outward unit normal vector, and σ is the surface tension of the liquid.

5. At the dynamic contact line (DCL), the stress singularity is removed by applying the Navier's slip condition (see for example[32]) and a constant contac angle is set:

$$(1/\beta)\mathbf{i} \cdot (\mathbf{v} - \mathbf{i}) = \mathbf{i} \cdot (\mathbf{T} \cdot \mathbf{n}) \tag{10}$$

$$\mathbf{n}_w \cdot \mathbf{n}_f = \cos(\theta_d), \tag{11}$$

where β is the slip coefficient, $\mathbf{n}_w$ is the normal vector to the solid wall directed into the fluid and $\mathbf{n}_f$ is the outward normal vector to the free surface

6. The DSCL is fixed at the edge of the die lip; then both x and y-coordinate are fixed

$$\mathbf{x}_{dscl} = \mathbf{x}_{edge} \tag{12}$$

7. Finally, the USCL is free to move along the die lip and therefore it have always the same y-coordinate

$$\mathbf{j} \cdot \mathbf{x}_{uscl} = 1 \tag{13}$$

We also set an upstream static contact angle, θ_s, as in Eq. (11).

2.2. Governing equations for particle transport

In this work we used the model proposed by Phillips et al.[11] to describe particle transport in the suspension flow. The model, in steady state condition, considers that particles are transported by convection and diffusion mechanisms. Then, the general conservation equation for the particle volume fraction is

$$\nabla \cdot (\phi \mathbf{v}) + \nabla \cdot (\mathbf{N}_t) = 0, \tag{14}$$

where $\mathbf{N}_t$ is the total particle flux that accounts for Brownian diffusion, sedimentation, shear and viscosity gradients induced transport. Under the hypothesis of non-colloidal suspension and neutrally buoyant particles, the first two mechanisms are neglected. Therefore, we only consider here the fluxes induced by shear rate and viscosity gradients, which according to Phillips et al.[11] are given by:

$$\mathbf{N}_t = \mathbf{N}_\phi + \mathbf{N}_\eta \tag{15}$$

$$\mathbf{N}_\phi = -k_c a^2(\phi^2\nabla\dot{\gamma} + \phi\dot{\gamma}\nabla\phi) \tag{16}$$

$$\mathbf{N}_\eta = -k_\eta\dot{\gamma}\phi^2\left(\frac{a^2}{\eta_r}\right)\frac{d\eta_r}{d\phi}\nabla\phi. \tag{17}$$

k_c and k_η are constants of order unity, which must be determined by experiments, a is the particle radius and $\dot{\gamma}$ is *the deformation rate* or simply *shear rate*.[33] It is defined as

$$\dot{\gamma} = \sqrt{\frac{1}{2}\mathrm{tr}(\underline{\underline{\dot{\gamma}}}^2)} = \tag{18}$$

$$= \left[2\left(\frac{\partial u}{\partial x}\right)^2 + 2\left(\frac{\partial v}{\partial y}\right)^2 + 2\left(\frac{\partial u}{\partial y} + \frac{\partial v}{\partial x}\right)^2\right]^{1/2} \tag{19}$$

The final transport equation is obtained after replacing Eqs. (15) to (17) in Eq. (14):

$$\mathbf{v}\cdot\nabla\phi = \nabla\cdot(\bar{D}\nabla\phi) + k_c a^2\nabla\cdot(\phi^2\nabla\dot{\gamma}), \tag{20}$$

where

$$\bar{D} = k_c a^2\phi\dot{\gamma} + k_\eta\dot{\gamma}\phi^2\frac{a^2}{\eta}\frac{d\eta}{d\phi} \tag{21}$$

The boundary conditions applied to solve Eq. (20) are:

1. At the feed slot, we consider a constant concentration profile with $\phi = \bar{\phi}$, where $\bar{\phi}$ the *average bulk concentration* of the suspension.
2. The solid walls are impermeable and then the particle flux is set to zero: $\mathbf{n} \cdot \mathbf{N}_t = 0$.
3. At the outflow plane, we impose a fully developed flow condition: $\mathbf{n} \cdot \mathbf{N}_t = 0$.
4. Finally, because in this work we do not consider adsorption/desorption at interfaces, the particle flux is also set to zero along the free surfaces.

In the finite element method, the velocity field is usually written as a linear combination of continuous piece-wise polynomials. Therefore, along element boundaries, the velocity $\mathbf{v}$ is continuous, but the velocity gradient $\nabla \mathbf{v}$ is not. Therefore, the weighted residual of the particle transport equation, which includes the integral of the gradient of deformation rate $\nabla \dot{\gamma}$ cannot be evaluated. A common approach to avoid this problem is to represent the velocity gradient as a separate independent field which is defined also as a linear combination of continuous piece-wise polynomials. Thus, an additional variable $\mathbf{G} = \nabla \mathbf{v}$ that is continuous between the elements is introduced and it is called *interpolated velocity gradient*. This is the same approach used in the solution of viscoelastic flows using finite element method (see Szadi et al.[34]).

The approximate solution satisfies the continuity equation only in an integral sense, $\mathrm{tr}(\mathbf{G}) = \nabla \cdot \mathbf{v} = 0$ is not satisfied in every point of the flow domain. Pasquali and Scriven[35] suggested that the interpolated velocity gradient field $\mathbf{G}$ can be defined such that the incompressibility constrain is automatically enforced, i.e. $\mathrm{tr}(\mathbf{G}) \equiv 0$. The proposed definition is:

$$\mathbf{G} - \nabla\mathbf{v} + \frac{\nabla\cdot\mathbf{v}}{\mathrm{tr}(\mathbf{I})}\mathbf{I} = \mathbf{0} \tag{22}$$

Note that $\mathrm{tr}(\mathbf{G}) = \mathrm{tr}(\nabla\mathbf{v}) - \nabla\cdot\mathbf{v} = 0$.

In the next section we present the numerical method used to discretize and solve the free boundary problem defined by Eqs. (1), (2), (20) and (22).

The governing equations are made dimensionless by using V_s, H_0, H_0/V_s and $V_s\eta_s/H_0$ as scales for velocity, length, time and stress, respectively.

3. Numerical Solution

3.1. Formulation of the free boundary problem

In coating flows, the domain Ω (with boundaries Γ) is unknown *a priori* due to the presence of the free surfaces. Thus, to solve this free boundary problem by standard techniques, the set of differential equations and boundary conditions have to be transformed to an equivalent set defined in a known reference domain $\overline{\Omega}$ (with boundaries $\overline{\Gamma}$). This can be done by using a mapping $\mathbf{x} = \mathbf{x}(\boldsymbol{\xi})$ between the two domains. The unknown physical domain is parameterized by the position vector $\mathbf{x}$ and the reference domain, by the vector $\boldsymbol{\xi} = (\xi, \zeta)$. The technique is described in detail in.[36] The main idea is to define an inverse mapping governed by a pair of elliptic differential equations that, when solved with appropriate boundary conditions, gives $\mathbf{x}$, the coordinates of the computational nodes in the spatial domain. Thus, the coordinates ξ and ζ of the reference domain satisfy

$$\nabla\cdot(\mathbf{D}\cdot\nabla\boldsymbol{\xi}) = 0, \tag{23}$$

where $\nabla \equiv \partial/\partial \mathbf{x}$ denotes differentiation in physical space, and $\mathbf{D}$ is the diffusivity-like adjustable tensor that serves to control the gradients in coordinate potentials, and thereby the spacing between curves of constant ξ and constant ζ. With this technique, free boundaries are implicitly defined in the reference domain as boundaries where special boundary conditions are used. For example, the position of the free surfaces is calculated by imposing the kinematic condition, e.g. Eq.(9). The solid walls and synthetic inlet and outlet boundary planes are specified as functions of the coordinates and along them stretching functions are used to distribute conveniently the constant coordinate curves. Dynamic and static contact angles are imposed by replacing one of the elliptic mesh generation equation on the contact line node by Eq. (11); the other equation is replaced by the correspondig displacement restriction (see for example Eqs. (13) and (12)). The discrete versions of the mapping Eq. (23) are generally referred to as *mesh generation equations*.

3.2. Discretization by the finite element method

The weighted residual equations are obtained after multiplying the governing Eqs. (1), (2), (20), (22) and (23) by appropriate weighting functions associated with each degree of freedom ψ_i^c, ψ_i^m, ψ_i^ϕ, ψ_i^G and ψ_i^x, respectively, integrating over the unknown flow domain Ω (bounded by Γ), applying the divergence theorem to the diffusion terms (those with divergence) and mapping the integrals onto the known reference domain $\overline{\Omega}$ (bounded by $\overline{\Gamma}$). Details of this process are well known and were presented by Romero et al.[37] Here, this procedure is shown in detail only for the particle transport equation. After multiplying Eq. (20) by ψ_i^ϕ, integrate it over the spatial domain Ω, applying the divergence theorem to the appropriate term and mapping the integral to the reference domain, the weigthed residual becomes:

$$\begin{aligned} R_i^{\phi} \equiv & \int_{\bar{\Omega}} \left[(\mathbf{v} \cdot \nabla \phi) \psi_i^{\phi} + (\bar{D} \nabla \phi \cdot \nabla \psi_i^{\phi}) + k_c a^2 \phi^2 (\nabla \dot{\gamma} \cdot \nabla \psi_i^{\phi}) \right] J d\bar{\Omega} \\ & - \int_{\bar{\Gamma}} \mathbf{n} \cdot \left[(\bar{D} \nabla \phi) + (k_c a^2 \phi^2 \nabla \dot{\gamma}) \psi_i^{\phi} \right] (d\Gamma / d\bar{\Gamma}) d\bar{\Gamma} = 0, \end{aligned} \tag{24}$$

$J = \det(\mathbf{J}) = d\Omega / d\bar{\Omega}$ is the determinant of the Jacobian mapping and $\mathbf{n}$ is the outward unit normal vector to the boundary Γ. Thus, the last integral represents the diffusive particle flux on the boundaries of the flow domain. With the imposed boundary conditions, it is zero everywere to enforce the zero flux condition on solid surfaces (impermeability), free surfaces (no adsorption/desorption) and in the cross section of the film thickness (fully developed concentration profile).

Each independent variable is approximated with a linear combination of a finite number of basis functions, Thus, $\mathbf{v} \approx \sum_i \bar{\mathbf{v}}_i \varphi_i^m$, $\mathbf{x} \approx \sum_i \bar{\mathbf{x}}_i \varphi_i^{\mathbf{x}}$, $\phi \approx \sum_i \bar{\phi}_i \varphi_i^{\phi}$, $\mathbf{G} \approx \sum_i \bar{\mathbf{G}}_i \varphi_i^G$ and $p \approx \sum_i \bar{p}_i \varphi_i^c$. The quantities with overbar represent the coefficients of the expansions, i.e. the unknown of the discrete problem. The basis functions used to expand the independent variables are: Lagrangian bi-quadratic polynomials for velocity φ_i^m, position $\varphi_i^{\mathbf{x}}$ and concentration φ_i^{ϕ}, Lagrangian bi-linear polynomials for the interpolated velocity gradient φ_i^G and linear discontinuous polynomials for pressure φ_i^c. The Galerkin method is applied to the equations of momentum, continuity, mesh generation and interpolated velocity gradient, i.e. $\psi_i^m = \varphi_i^m$, $\psi_i^c = \varphi_i^c$, $\psi_i^{\mathbf{x}} = \varphi_i^{\mathbf{x}}$, $\psi_i^{\mathbf{G}} = \varphi_i^{\mathbf{G}}$. Streamline Petrov-Galerkin is applied to the particle transport equation, i.e. $\psi_i^{\phi} = \varphi_i^{\phi} + h\mathbf{v} \cdot \nabla \varphi_i^{\phi}$. After replacing the interpolated variables in the corresponding weigthed residuals, the system of partial differential equations reduces to a simultaneous algebraic non-linear equations system for the coefficients of the basis functions of all fields.

A mesh with $1,312$ quadrilateral elements was used in all the results reported here. Increasing the number of elements by 50% in each direction did not significantly change the concentration and velocity profiles under the downstream die lip and coated film.

3.3. Solution of the non-linear system and validation

The system of equations was solved simultaneously for all variables using Newton's method. The entries of the Jacobian matrix $\mathbf{J}$ were evaluated numerically using a central finite difference scheme.[37] In each iteration the linearized equation system was factorized into unit lower $\mathbf{L}$ and upper $\mathbf{U}$ triangular matrices by a frontal solver. In order to assure the convergence of the Newton loop within 6 to 8 iterations, at each successive set of operating conditions (parameters), the initial guess was generated by a pseudo-arc-length continuation method.[38] The tolerance on the L2-norm of the residual vector and on the last Newton update of the solution was set to 10^{-6}.

To validate the model and the implementation, predictions were compared to the analytical solution of the fully developed, pressure driven particle suspension flow between parallel plates. As shown by Phillips et al.,[11] an analytical form for the velocity and concentration profiles can be obtained for the particular case of $k_c/k_\eta = 0.65$. The concentration profile is:

$$\phi = \frac{1}{1 + \frac{(1-\phi_w)y}{\phi_w}} , \tag{25}$$

where ϕ_w is the dimensionless particle concentration at the channel wall and y is the vertical coordinate in units of the channel half width H. On the symmetry line ($y = 0$), $\phi = 1$, because particles migrate towards the zero-shear rate region until the maximum packing concentration is reached. The velocity profile is then obtained by numerical integration (using trapezoidal rule) of the following expression:

$$u(y) = u^*(y)/u_{max} = 1 - \frac{dp}{dz}\frac{H^2}{2\eta_s u_{max}} \int_0^y \frac{y}{(1-\phi)^{-1.82}} dy, \qquad (26)$$

where ϕ is given by Eq. (25).

The conditions of the problem used in the validation were: $L/H = 10$ and $\bar{\phi} = 0.59$. A parabolic velocity profile and a uniform concentration distribution were imposed in the inflow. In the outflow plane, we assumed a fully developed flow. Figure 2 shows the particle concentration field; as expected, the concentration near the wall, where the shear rate is high, is low and near the center line is high; that is, particles migrate from the high shear region towards the low shear region. Figure 3 depicts the particle concentration along both the centerline and channel wall. The results show that the channel length was long enough to reach the fully developed profiles at the exit plane. The particle distribution became fully developed (independent of x) at $x \approx 6H$. This entrance length is smaller than the one estimated by the scaling analysis presented by Nott and Brady.[18] With the set of parameters used in this validation case, the estimated entrance length should be $L_e \approx 40H$. We are not sure the reason for this difference. One possible explanation is that the scaling arguments used to estimate the entry length considers a shear-induced diffusion coefficient $D \approx \phi\dot{\gamma}a^2$, this corresponds

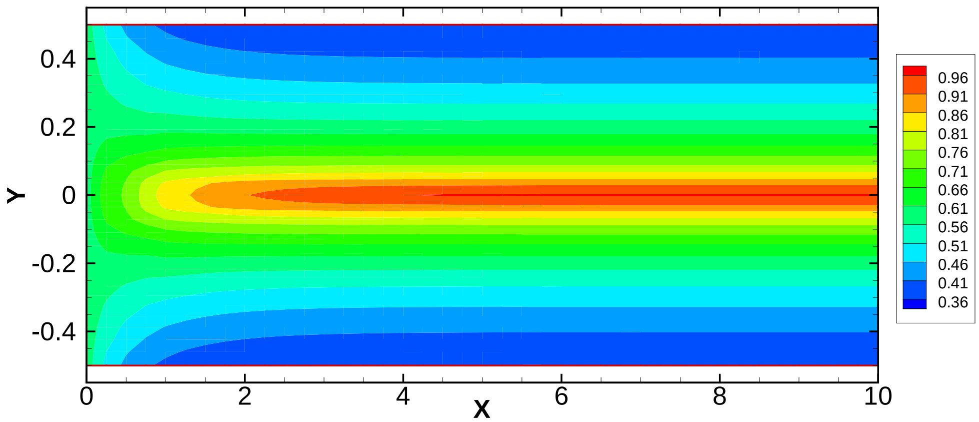

Figure 2: Particle concentration field in the supension inside a rectangular channel. On the left, a uniform concentration $\bar{\phi} = 0.59$ and a velocity profile given by Eq. (26) are imposed.

to the second term of eq.16. However, the total particle flux includes a second term, which accelerates the particle transport toward the center of the channel and should reduce the entrance length.

The computed velocity and concentration profiles at the outflow plane were compared to the fully-developed analytical solution in Figure 4. The agreement between the numerical prediction and exact solution is very good, showing a maximum error equal to 3.4% at the center line. This discrepancy is associated with the singularity at the symmetry line as explained below.

The diffusive flux model predicts particle migration towards regions where the deformation rate is low, that is, the symmetry line in this case. Actually, the simulations predicts values as high as $\phi = 1$, i.e. the maximum packing concentration. As $\phi \to 1$ the viscosity approaches infinity (see Eq. (4)), the Jacobian matrix becomes singular and the Newton's method fails. The

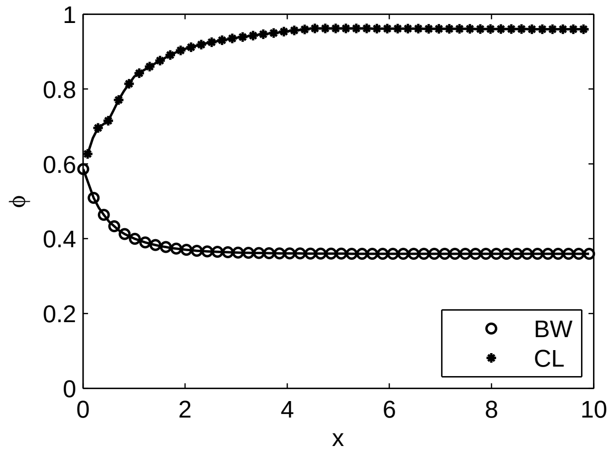

Figure 3: Particle concentration along the x-coordinate on the center line (CL) and bottom wall (BW) for the rectangular channel case shown in Figure 2.

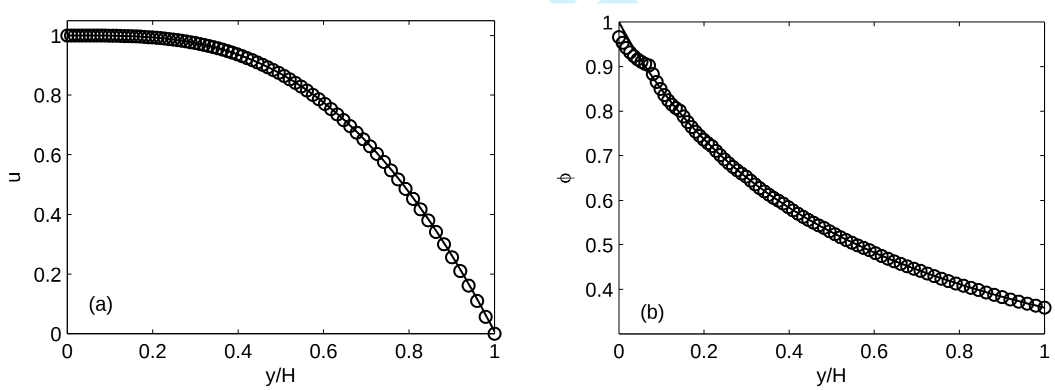

Figure 4: Comparison of the numerical results with the exact solution at the exit of the rectangular channel: a) velocity profile and b) concentration profile. In both cases, the continuous lines correspond with exact solution of the Eqs. (25) and (26).

singularity was avoided by using a strategy based in the concept of the *non-local stress* developed by Nott and Brady[18] and Miller and Morris.[39] At the particle scale, the continum hypothesis is not valid and the deformation rate is not correctly represented by $\underline{\underline{\dot{\gamma}}}$. As discused by Miller and Morris,[39] different approaches can be implemented to model this non-local stress but the main idea is that the shear rate at particle level is higher than the continuous representation and never goes exactly to zero. A small non-local shear rate value $\dot{\gamma}_{NL}$, which is a function of the particle size, is added to the local shear rate:

$$\dot{\gamma}_{NL} = a_s U_{loc}/l, \tag{27}$$

where $a_s = (a/l)^2$, l is the channel width and U_{loc} is the local fluid velocity (see Miller & Morris [41]). Thus, when Eq. (27) is added to the local deformation rate (Eq. (19)), the non-zero shear rate avoids the concentration reaching the maximum packing value.

4. Results

The flow under the downstream die lip is almost rectilinear and is well approximated by a superposition of Couette (substrate drag) and Poiseuille (pressure driven) flows. The pressure gradient is directly related to the imposed flow rate (film thickness).[40,41,42,43] For Newtonian flow, at a film thickness $t = t^*/H = 1/2$, the pressure gradient under the downstream die lip vanishes, the velocity profile is linear and the shear rate gradient is zero. At lower film thickness, an adverse pressure gradient occurs to counter act the drag from the substrate. At $t = 1/3$, the shear rate at the die surface vanishes. At even lower flow rate, flow reversal occurs near the die surface and a recirculation appears. Since particle migration is driven by shear rate gradient, the final particle distribution in the coated layer should be strongly affected by the imposed film thickness.

In this work, the flow topology and particle distribution are analyzed at three different values of the film thickness, e.g. $t = 0.5$, $t = 0.37$ and $t = 0.14$. The flow of the particle suspension is compared to the equivalent case at which particle migration is not taken into account and the viscosity of the liquid is constant throughout the flow (equal the viscosity of the suspension at the average bulk particle concentration).

Table 1 shows the values of the dimensional parameters used in this study. The corresponding capillary number is $Ca = 0.1$. The values of the coefficients of the diffusive flux model (k_c and k_η) were in the same order of the experimental values determined by Phillips et al.[11]

4.1. Flow state at $t/H_0 = 0.5$

As was mentioned before, the pressure gradient under the die lip vanishes for Newtonian flow at $t/H_0 = 0.5$, and the flow is well approximated by a pure Couette flow. This imply that the shear rate is almost constant in this region. Figure 5-a shows the particle concentration field for this condition. In the feed slot, particles migrate towards the symmetry plane, from the high shear region near the wall towards the low shear region in the symmetry plane. At the exit of the feed slot, the concentration at the center of the channel is close to the maximum packing concentration.

Detail of the particle concentration field in the upstream part of the coating bead is presented in Figure 5-b. The particle concentration near

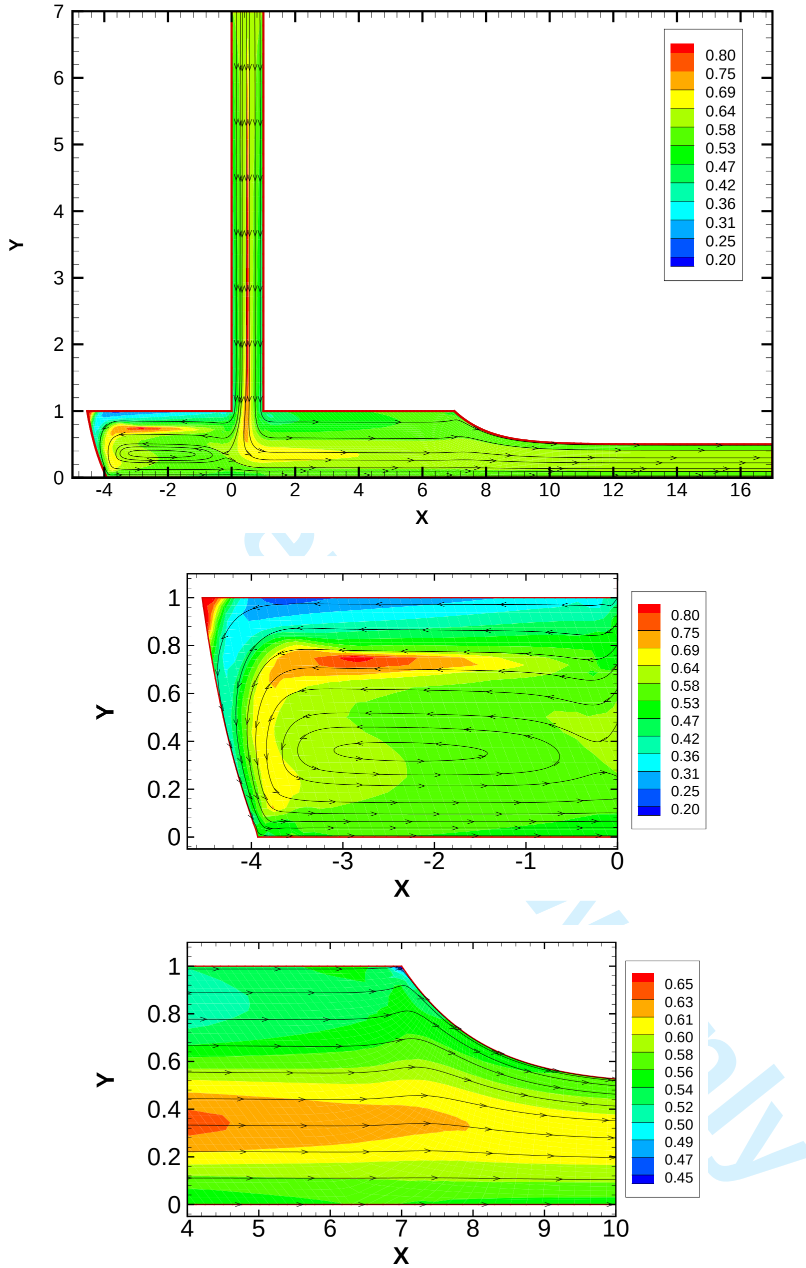

Figure 5: a) Particle concentration field and selected streamtraces in the domain, for the parameters listed in Table 1. b) Zoom on the upstream slot coating region, showing the region of high particle concentration near the upstream static contact line. c) Zoom of the downstream slot coating region.

V_s	0.1 $[m/s]$
P_{vac}	-3.7 $[kPa]$
σ	0.06 $[N/s]$
η_s	0.06 $[Pa\, s]$
a	4 $[\mu m]$
H_s	10^{-4} $[m]$
H_0	10^{-4} $[m]$
$\bar{\phi}$	0.59
k_c	0.816
k_η	1.22

Table 1: Values of the parameters used in the simulation with $t = 0.5$

the die lip is low, because particles migrate from this high shear rate zone close to the die surface towards a low shear rate region near a layer where the deformation rate almost vanishes ($y \sim 0.7$).

The correct description of the effect of vacuum pressure on the upstream meniscus position needs to take into account that the viscosity of the liquid attached to the die lip is lower than the viscosity at the average particle concentration. Figure 6 presents the pressure along the substrate in the upstream bead for the flow of a particle suspension and the equivalent Newtonian flow that does not take particle migration into account. In the later, the liquid viscosity was set at the value of the average concentration, $\bar{\phi} = 0.59$, and was constant throughout the flow; e.g. $\eta_r(\bar{\phi}) = 5.3$. The lower viscosity of the liquid attached to the substrate and die lip reduces the necessary ad-

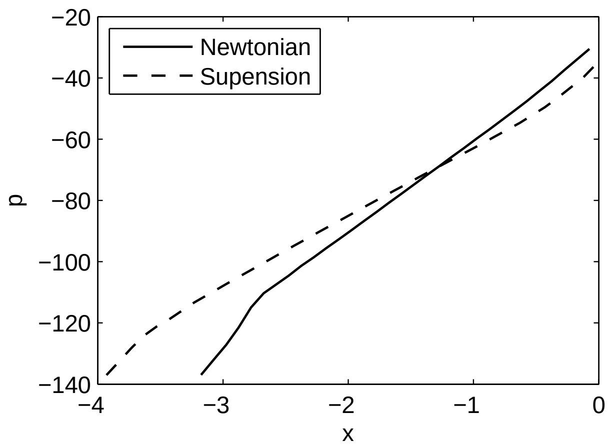

Figure 6: Pressure on the moving substrate in the upstream region, for the conditions of Table 1 (Suspension) and the same parameters but without particle migration (Newtonian).

verse pressure gradient to counteract the drag by the substrate. Therefore, for a fixed vacuum pressure, the meniscus is located further away from the feed slot. Although not explored here, the lower and upper vacuum pressure operability limits in slot coating window (see Carvalho and Keshghi[41]) are modified when particle transport is taken into consideration in the model.

Figure 5 shows that for these conditions, the high particle concentration near the center of the feed slot is convected through the downstream coating bead with weak particle diffusion, leading to high particle concentration in a layer located at $y \sim 0.4$. For $t = 0.5$, the velocity profile under the downstream die lip is close to a linear profile (Couette flow), as show in Figure 7-a. The shear rate is almost constant and particle migration is only driven by viscosity gradient, that forces particle to diffuse from high viscosity (high concentration) regions to lower viscosity (low concentration) regions.

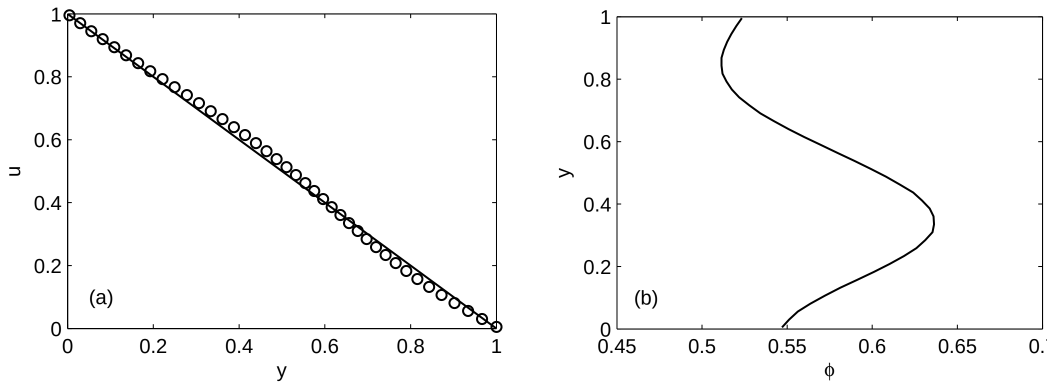

Figure 7: Velocity (a) and concentration (b) profiles at $x \sim 4$ for the case with $t = 0.5$ (Figure 5). The theoretical profile of a Coutte flow is also included for comparison (continuous line in frame (a)).

However, at the conditions analyzed, this effect is weak and the concentration profile at $x \sim 4$ (middle of downstream lip) shows a layer of higher particle concentration ($\phi \sim 0.65$) at $y \sim 0.4$.

The concentration field near the downstream free surface is shown in Figure 5-c. Close to the static contact line, the deformation rate is high leading to a region of low particle concentration ($\phi \sim 0.4$). The layer of high particle concentration remains in the final film, as shown in Figure 8. The concentration at the substrate and at the free surface ($\phi \approx 0.56$) are lower than the average particle concentration $\bar{\phi} = 0.59$ and there is a layer of higher particle concentration ($\phi \approx 0.61$) located approximately in the middle of the coated layer.

4.2. Flow state at $t/H_0 \sim 1/3$

As discussed before, at $t/H_0 = 1/3$ and constant viscosity, the adverse pressure gradient is such that the deformation rate vanishes at the down-

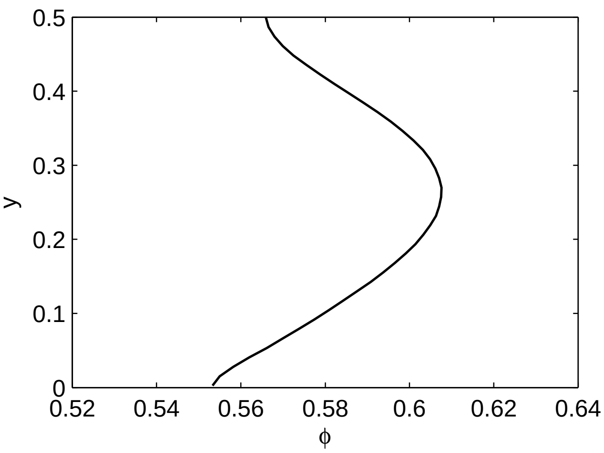

Figure 8: Concentration profile along the cross section of the coated film ($x = 17$).

stream slot die wall. According to the diffusive flux model, particles will migrate towards this region. The non-uniform shear rate flow completely changes the particle concentration field in the downstream coating bead and on the final coated film, when compared to the case at $t/H_0 = 0.5$.

In this section, the flow field at $t/H_0 = 0.37$ is presented. At this condition, the zero shear rate is not located exactly at the wall, but very close it. The flow (represented by streamtraces) and particle concentration field are presented in Figure 9-a. The upstream flow and particle distribution pattern (Figure 9-b) are similar to that presented in Figure 5-b (at $t/H_0 = 1/2$). By contrast, the downstream behavior presented in Figure 9-c is quite different. A high particle concentration region is formed close to the dip lip surface. The velocity and concentration profile across the coating gap at $x \sim 4$ is shown in Figure 10. The low shear rate close to the die wall and corresponding high particle concentration is clearly observed. The high particle concentration layer is convected to the top of the coated film. The concentration profile across the thickness of the coated layer is shown in Figure 11. Now, the particle concentration on the free surface ($\phi \sim 0.62$) is higher than the average concentration, $\bar{\phi} = 0.59$. This can have a tremendous effect on the drying process and particle structure formation.

4.3. Flow state at $t/H_0 < 1/3$

At film thickness lower than 1/3 of the coating gap, i.e. $t/H_0 < 1/3$, the adverse pressure gradient under the downstream die lip is strong enough that a recirculation is formed. This session presents results at very thin films, $t = 0.14H_0$, with $k_c = 0.34$ and $k_\eta = 0.51$. The coefficients of the diffusive flux model were changed because it was not possible to obtain converged solution for the values of Table 1. We infer that the convergence problems were associated to the high concentration gradients associated to particle accumulated inside the recirculation, which are very steep to be capture by our mesh refinement.

The flow and particle concentration field are shown in Fig. 12. The recirculation under the die lip has a strong effect on the particle distribution in the coating bead, because a region of high particle concentration is formed inside the recirculation. The backflow creates a layer of maximum negative velocity and vanishing shear rate towards which particles migrate. This high particle concentration inside a vortex may promote particle aggregation which is usually undesired. Because of the large recirculation, all the liquid comming from the feed slot flows back to the upstream bead before being dragged by the substrate. The high particle concentration layer at the center of the feed is re-distributed in this process and, due to particle migration from the substrate, a layer with higher concentration is created close the flow separating

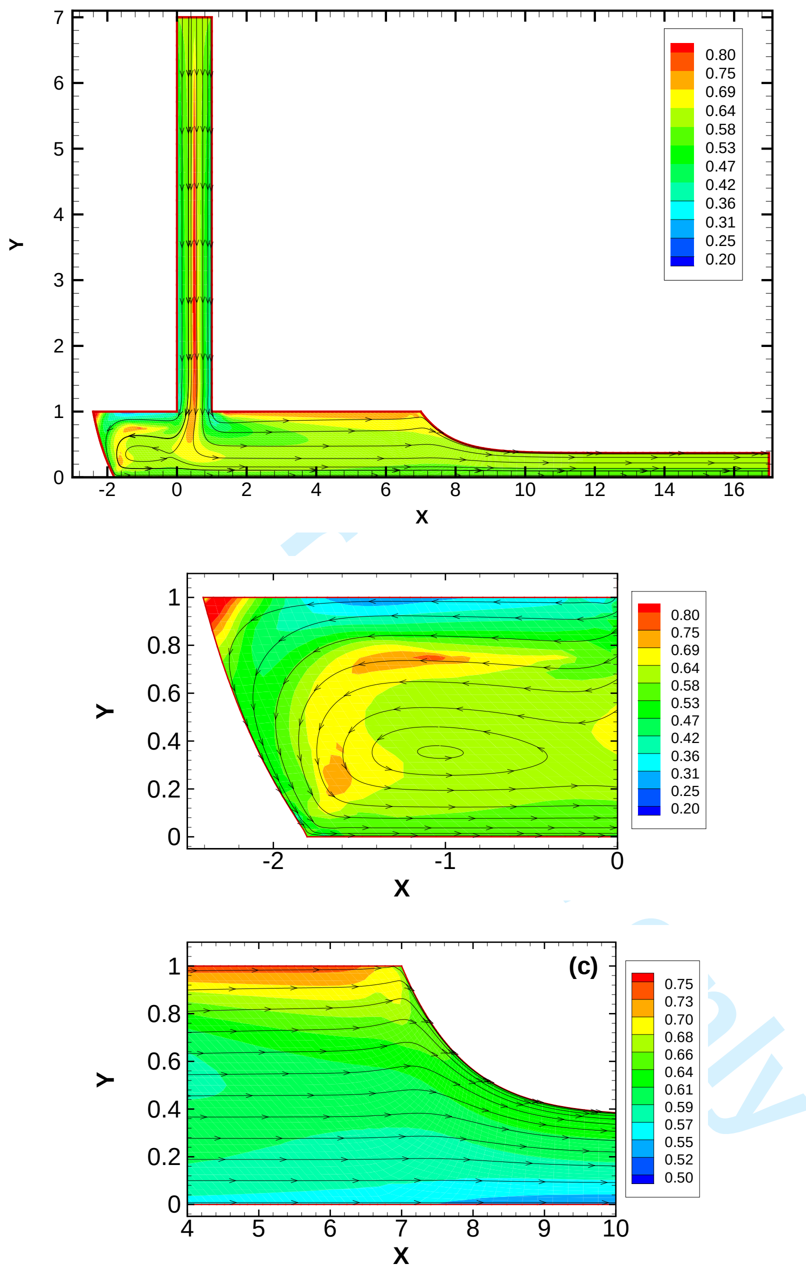

Figure 9: As in Figure 5 but for $t = 0.37$.

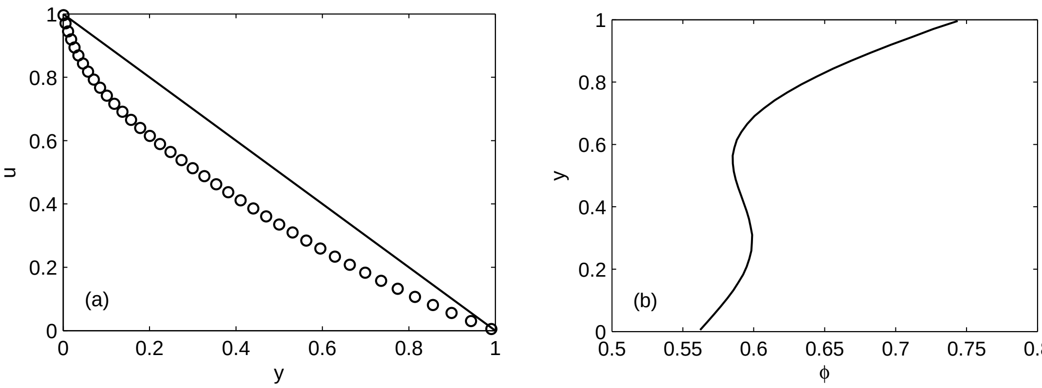

Figure 10: Velocity (a) and concentration (b) profiles at $x \sim 4$ for the case with $t = 0.37$ (Figure 9). The theoretical profile of a Coutte flow is also included for comparison (continuous line in frame (a)).

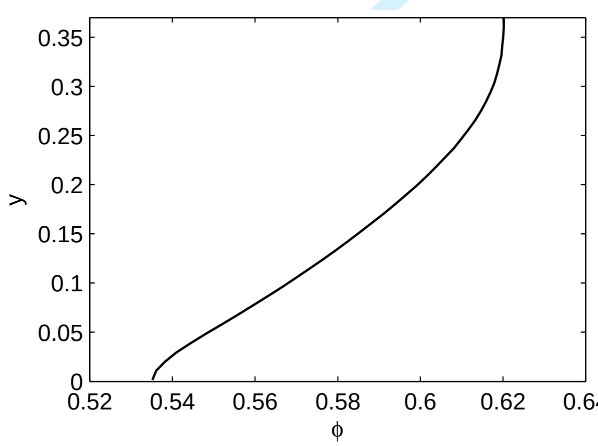

Figure 11: Concentration profile along the cross section of the coated film ($x = 17$), for $t = 0.37$.

streamline that terminates at the meniscus stagnation point. This explains the shape of the profile across the coated film as presented in Fig.13. The particle distribution is similar to the one obtained at $t = 0.37$ with the high concentration at the top of the film ($\phi \sim 0.62$) and low ($\phi \sim 0.54$) at the substrate.

5. Final Remarks

Slot coating flow of non-colloidal particle suspensions was studied to determine the effect of operating conditions on the particle distribution in the coating bead and deposited liquid layer. The flow was described by the mass and momentum conservation equations coupled with a particle transport equation based on the diffusive flux model proposed by Phillips et al.[11] The viscosity was considered a function of the local particle concentration and independent of the local shear rate. The problem was discretized using the finite element method and the unknown domain and free surface was mapped with an elliptic mesh generation technique. The resulting set of algebraic nonlinear equations was solved using the Newtons method.

The results show that the particle distribution in the coating bead is non-uniform. The complex flow field leads to shear induced particle transport. Since the deformation rate field is strongly dependent on the imposed flow rate (wet thickness), the particle distribution in the flow and consequently in the coated layer drastically changes as the film thickness varies. When the film thickness is 1/2 of the coating gap, the shear under the downstream die lip is almost constant and the high particle concentration region formed in the center of the feed slot is convected, leading to a high particle concentration

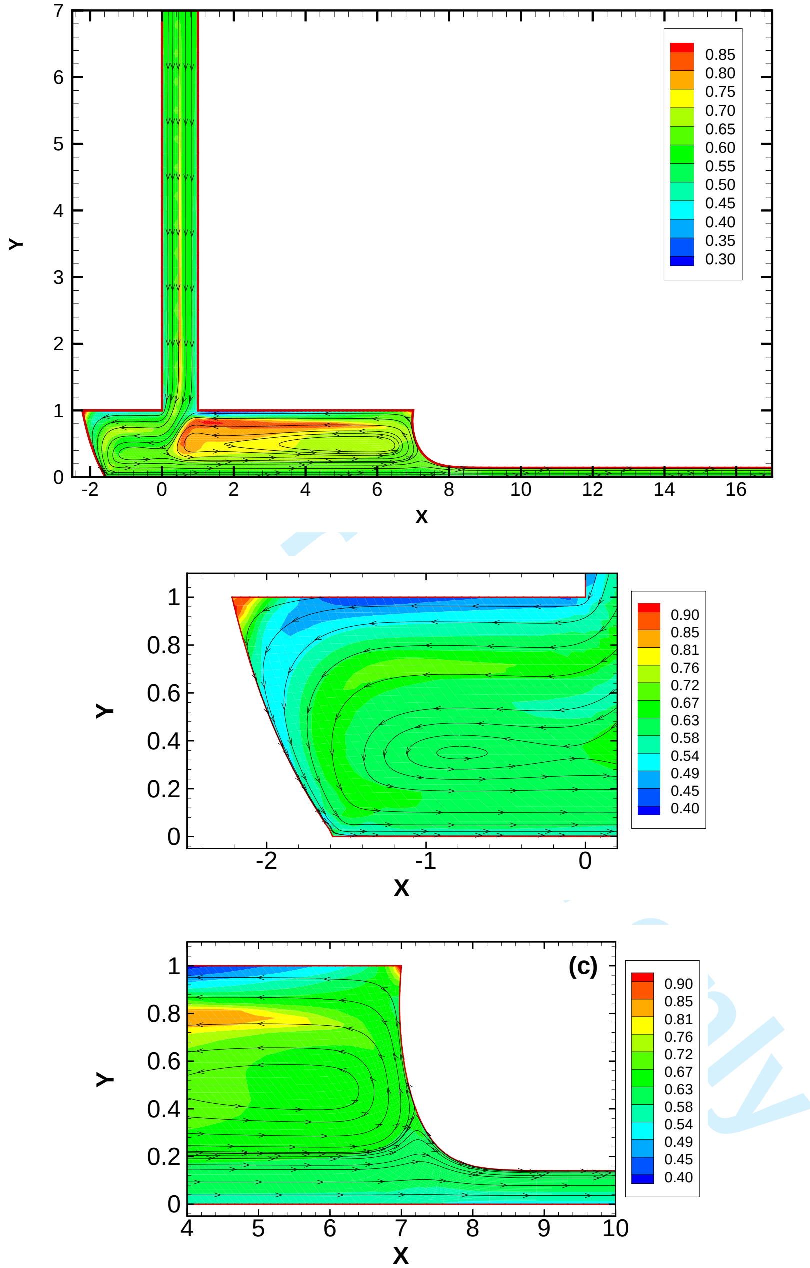

Figure 12: As in Figure 5 but for $t = 0.14$.

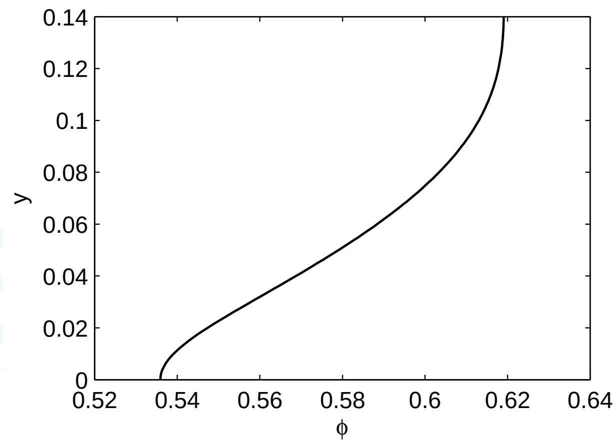

Figure 13: Concentration profile along the cross section of the coated film ($x = 17$), for $t = 0.14$.

layer in the middle of the coated film. At a film thickness close to 1/3 of the coating gap, particles are transported towards the zero-shear region close to the die lip, leading to high particle concentration in the die surface and on the surface of the coated layer. The high concentration in the die lip may have a strong effect on particle agglomeration and streak formation that ultimately leads to coating defects. At even lower flow rates, particles accumulate inside the flow recirculation, which also may lead to undesirable agglomeration and coating defects.

Although experimental results on particle distribution in the liquid layer deposited using slot coating is not available, it is clear that is has a strong effect on the flow and drying processes, and microstructure formation. The effect of particles in the coating liquid on the operability limits of the process has been reported.[44]

The results presented here show that process conditions (wet thickness) can be used to obtain the desired particle distribution. The two-dimensional, steady-state flows can be used as base state for stability analysis, to determine the conditions at which the flow ceases to be two-dimensional and steady, which are usually associated with process limits.[41]

A natural extension of the model is to consider particles that are not neutrally buoyant and the surface tension as a function of local particle concentration.[45] The present results shown high concentration gradients at the downstream interface that may generate strong Marangoni stresses if the surface tension varies locally with the particle concentration. This tangential stresses could have a deep impact on the flow field,[46] the interface shape and, consequently on the operability window of the process.

Acknowledgments

The authors would like to thank to the following institutions for financial support: *Fundação de Amparo à Pesquisa do Estado do Rio de Janeiro* (FAPERJ), *Conselho Nacional de Desenvolvimento Científico e Tecnológico* (CNPq-Brazil), *Consejo Nacional de Investigaciones Científicas y Técnicas* (CONICET-Argentina) and the program *Industrial Partnership for Research in Interfacial and Material Engineering* (IPRIME) of the University of Minnesota.

References

[1] Cardinal CM, Jung YD, Ahn KH, Francis LF. Drying regime maps for particulate coatings. *AIChE Journal* 2010; **56**(11):2769–2780.

[2] Chang CY, Powell RL. Hydrodynamic transport properties of concentrated suspensions. *AIChE Journal* 2002; **48**:2475–2480.

[3] Stickel JJ, Powell RL. Fluid mechanics and rheology of dense suspensions. *Annual Review of Fluid Mechanics* 2005; **37**:129–449.

[4] Santamaria-Holek I, Mendoza CI. The rheology of hard sphere suspensions at arbitrary volume fractions: an improved differential viscosity model. *Journal of Chemical Physics* 2009; **130**(044904):1–7.

[5] Shewan HM, Stokes JR. Analytically predicting the viscosity of hard sphere suspensions from the particle size distribution. *Journal of Non-Newtonian Fluid Mechanics* 2015; **222**:79–81.

[6] Karnis A, Goldsmith AL, Mason SG. The kinetics of flowing dispersions: concentrated suspensions of rigid particles. *Journal of Non-Newtonian Fluid Mechanics* 1966; **22**:531–553.

[7] Gadala-Maria F, Acrivos A. Shear-induced structure in a con-centrated suspension of solid spheres. *Journal of Rheology* 1980; **24**:799–814.

[8] Leighton D, Acrivos A. Measurement of shear-induced self-diffusion in concentrated suspensions of spheres. *J. Fluid Mechanics* 1987; **177**:109–131.

[9] Graham AL, Altobelli SA. NMR imaging of shear-induced diffusion and structure in concentrated suspensions. *Journal of Rheology* 1991; **35**:191–201.

[10] Altobelli SA, Givler RC. Velocity and concentration measure-ments of suspensions by nuclear magnetic resonance imaging. *Journal of Rheology* 1991; **35**:721–734.

[11] Phillips RJ, Armstrong RC, Brown RA, Graham AL, Abbott JR. A constitutive equation for concentrated suspensions that accounts for shear-induced particle migration. *Physics of Fluids A: Fluid Dynamics* 1992; **4**(1):30–40.

[12] Chow AW, Sinton SW, Iwamiya JH, Stephens TS. Shear-induced migration in couette and parallel-plate viscometers: NMR imaging and stress measurements. *Physics of Fluids* 1994; **6**:2561–2576.

[13] Hampton RE, Mammoli AA, Graham AL, Tetlow N, Altobelli SA. Migration of particles undergoing pressure-driven flow in a circular conduit. *Journal of Rheology* 1997; **41**:621–640.

[14] Subia SR, Ingber MS, Mondy LA, Altobelli SA. Modelling of concentrated suspensions using a continuum constitutive equation. *Journal of Fluid Mechanics* 1998; **373**:193–219.

[15] Krishnan GP, Beimfohr S, Leighton D. Shear-induced radial segregation in bidisperse suspensions. *Journal of Fluid Mechanics* 1996; **321**:371–393.

[16] Kim JM, Lee SG, Kim C. Numerical simulations of particle migration in suspension flows: frame-invariant formulation of curvature-induced migration. *Journal of Non-Newtonian Fluid Mechanics* 2008; **150**:172–176.

[17] Tetlow N, Graham AL, Ingber MS, Rubia SR, Mondy LA, Altobelli SA. Particle migration in a couette apparatus: experiment and modeling. *Journal of Rheology* 1998; **42**:307–327.

[18] Nott PR, Brady JF. Pressure-driven flow of suspensions: simulation and theory. *Journal of Fluid Mechanics* 1994; **275**:157199.

[19] Ritz JB, Bertrand F, Thibault F, Tanguy PA. Shear-induced particle migration in a short-dwell coater. *Chemical Engineering Science* 2000; **55**:4857–4867.

[20] Rao RR, Mondy LA, Altobelli SA. Instabilities during batch sedimentation in geometries containing obstacles: A numerical and experimental study. *International Journal of for Numerical Methods in Fluids* 2007; **55**:723–735.

[21] Ahmed GMY, Singh A. Numerical simulation of particle migration in asymmetric bifurcation channel. *Journal of Non-Newtonian Fluid Mechanics* 2011; **166**:42–51.

[22] Chong JS, Christiansen EB, Baer AD. Rheology of concentrated suspensions. *Journal of Applied Polymer Science* 1971; **15**(8):2007–2021.

[23] Metzner AB. Rheology of suspensions in polymeric liquids. *Journal of Rheology* 1985; **29**(6):739–775.

[24] Mewis J, Frith WJ, Strivens TA, Russel WB. The rheology of suspensions containing polymerically stabilized particles. *AIChE Journal* 1989; **35**(3):415–422.

[25] Furusawa T, Smith JM. Fluid-particle and intraparticle mass transport rates in slurries. *Industrial and Engineering Chemistry Fundamentals* 1973; **12**(2):197–203.

[26] Lenoble M, Snabre P, Pouligny B. The flow of a very concentrated slurry in a parallel-plate device: Influence of gravity. *Physics of Fluids* 2005; **17**(7):073303.

[27] Timberlake BD, Morris JF. Concentration band dynamics in free-surface couette flow of a suspension. *Physics of Fluids* 2002; **14**(5):1580–1589.

[28] Furbank RJ, Morris JF. An experimental study of particle effects on drop formation. *Physics of Fluids* 2004; **16**(5):1777–1790.

[29] Apostolou K, Hrymak AN. Discrete element simulation of liquid-particle flows. *Computers & Chemical Engineering* 2008; **32**(4-5):841–856.

[30] Min KH, Kim C. Simulation of particle migration in free-surface flows. *AIChE Journal* 2010; **56**(10):2539–2550.

[31] Krieger IM. Rheology of monodispersed latices. *Advances in Colloid and Interface Science* 1972; **3**(2):111–136.

[32] Huh C, Scriven LE. Hydrodynamic model of steady movement of a solid/liquid/fluid contact line. *J. Colloid Interface Sci.* 1971; **35**:85–101.

[33] Bird RB, Armstrong RC, Hassager O. *Dynamics of polymeric liquids: Fluid mechanics*, vol. 1. John Wiley & Sons, New York, USA, 1977.

[34] Szadi M, Salmon T, Liu A, Bornside D, Armstrong R. New mixed finite element method for viscoelastic flows governed by differential constitutive equations. *Journal of Non-Newtonian Fluid Mechanics* 1995; **59**:215–243.

[35] Pasquali M, Scriven LE. Free surface flows of polymer solutions with models based on the conformation tensor. *Journal of Non-Newtonian Fluid Mechanics* 2002; **108**:363–409.

[36] Christodoulou KN, Kistler SF, Schunk PR. *Advances in computational methods for free-surface flows.* Chapman Hall, London, UK, 1997.

[37] Romero OJ, Carvalho MS, Scriven LE. Slot coating of mildly viscoelastic liquids. *Journal of Non-Newtonian Fluid Mechanics* 2006; **138**:6375.

[38] Chang TFC, Keller HB. Arc-length continuation and multi-grid techniques for nonlinear elliptic eigenvalue problems. *SIAM J. ScI. Stat. Comput.* 1982; **3**(2):173194.

[39] Miller RM, Morris JF. Normal stress-driven migration and axial development in pressure-driven flow of concentrated suspensions. *Journal of Non-Newtonian Fluid Mechanics* 2006; **135**(2-3):149165.

[40] Sartor L. Slot coating: Fluid mechanics and die design. PhD Thesis, University of Minnesotta 1999.

[41] Carvalho MS, Kheshgi HS. Low-flow limit in slot coating: Theory and experiments. *AIChE Journal* 2000; **46**(10):1907–1917.

[42] Lee AG, Shaqfeh ESG, Khomani B. A study of viscoelastic free surface flows by the finite element method: Hele-shaw and slot coating flows. *Journal of Non-Newtonian Fluid Mechanics* 2002; **108**(1-3):327362.

[43] Romero O, Suszynski W, Scriven L, Carvalho M. Low-flow limit in slot coating of dilute solutions of high molecular weight polymer. *Journal of Non-Newtonian Fluid Mechanics* 2004; **118**(23):137 – 156.

[44] Chu WB, Yang JW, Wang YC, Liu TJ, Tiu C, Guo J. The effect of inorganic particles on slot die coating of poly(vinyl alcohol) solutions. *Journal of Colloid and Interface Science* 2006; **297(1)**:215–225.

[45] Binks BP. Particles as surfactant: similarities and differences. *Current Opinion in Colloid & Interface Science* 2002; **7**:21 – 41.

[46] Campana DM, Ubal S, Giavedoni MD, Saita FA. Numerical prediction of the film thickening due to surfactants in the Landau−Levich problem. *Phys. Fluids* 2010; **22**:032 103.